ScienceDirect

OpenNano

Open access

17.3
CiteScore

Submit your article | Guide for authors

Menu | Search in this journal

About the journal

OpenNano is an internationally peer-reviewed and open-access journal publishing high-quality original research articles and reviews focusing on the **application of nanoscience and nanotechnology, with an emphasis on conceptual novelty and scientific quality**.
OpenNano publishes research from basic to ...

View full aims & scope

Article publishing option

Open Access

Article Publishing Charge (APC): USD 2,980 (excluding taxes).
This journal is taking part in the GPOA program.
Review this journal's open access policy.

Compare APCs for other journal...

1 day
Submission to first decision

29 days
Submission to decision after review

63 days
Submission to acceptance

2 days

View all insights

Acceptance to online publication

Editor in Chief | View full editorial board

Professor Luca Casettari, PhD

University of Urbino, Urbino, Italy

Articles

Latest published | Top cited | Most downloaded | Most popular

Research article *Open access*

Sericin-Capped Gold Nanoparticles as a Potential Antimicrobial in Human Urine through Disrupting Bacterial Membranes and Changing Metabolism

Wararat Chiangjong, ... Pokket Sirisreetreerux

September 2026

View PDF

Research article *Open access*

Boronic acid and piperine-derived Carbon dots for inhibition and eradication of bacterial biofilm

Remya Radha, Mohammad H. Al-Sayah

September 2026

View PDF

Research article *Open access*

Electrostatically tunable metronidazole-loaded chitosan/pectin polyelectrolyte complex nanoparticles: Charge ratio–dependent self-assembly and drug delivery performance

Chutima Sinsuebpol, Sucharat Limsitthichaikoon

September 2026

View PDF

Research article *Open access*

Process intensification of lipid nanoparticle manufacturing via vortex-enhanced flow synthesis: from design to functional mRNA delivery

Kittipat Suwanpitak, ... Kampanart Huanbutta

September 2026

View PDF

Research article *Open access*

Polymer-capped iron oxide nanoparticles: Influence on physicochemical properties and antibacterial efficacy

Karina Citra Rani, ... Dwi Setyawan

September 2026

View PDF

Review article *Open access*

Anti-obesity therapeutics through the application of nanostructures in murine models: a systematic review

Rogelio González-Arellanes, ... Marco Antonio Rito Palomares

September 2026

View PDF

Review article *Open access*

Stimuli-responsive nanoparticles in 3D–4D printing for drug delivery: practical considerations and challenges in clinical translation

Isra Dmour, ... Eqbal Abu-Alkebash

September 2026

View PDF

Research article *Open access*

Elucidating the role of process and material parameters in the optimization of Soluplus®-based ketoprofen nanosuspensions using precipitation-ultrasonication method - a strategy for enhanced dissolution behavior

Alaa Abuawad, ... Shatha Alshaer

July 2026

View PDF

Read latest issue

Special issues and article collections

Responsive nanoparticles in drug delivery systems

Edited by Assoc. Professor Filippo Rossi, Yuta Kurashina, Fabio Pizzetti

24 November 2025

Nanomaterials and nano architectures for cancer application: from diagnostics to therapy

Edited by Prof. Dr. Stefano Cinti, Dr. Sima Singh, Dr. Numan Arshid

17 November 2025

Application of microfluidic technologies in pharmaceutical sciences

Edited by Luca Casettari, Mattia Tiboni

15 April 2023

Development of nucleic acid nanoparticles for gene therapy

Edited by Fengqiao Li

15 March 2023

View all special issues and article collections

View all issues

Online ISSN: 2352-9520

For authors

Resources for authors ↗

Track your accepted paper ↗

Journal Finder ↗

Researcher Academy ↗

Rights and permissions ↗

Journal Article Publishing Support Center ↗

For editors

Resources for editors ↗

Publishing Ethics Resource Kit ↗

Guest editors ↗

For reviewers

Resources for reviewers ↗

Reviewer recognition ↗

Volume 31

In progress (September 2026)

This issue is in progress but contains articles that are final and fully citable.

Nanomaterials and nano architectures for cancer application: from diagnostics to therapy

Article 100317

View PDF Article preview

Research article *Open access*

Process intensification of lipid nanoparticle manufacturing via vortex-enhanced flow synthesis: from design to functional mRNA delivery

Kittipat Suwanpitak, Tanikan Sangnim, Pattaravadee Srikoon, Chonlada Panpipat, ... Kampanart Huanbutta

Article 100319

View PDF Article preview

Research article *Open access*

Polymer-capped iron oxide nanoparticles: Influence on physicochemical properties and antibacterial efficacy

Karina Citra Rani, Agnes Nuniek Winantari, Tahta Amrillah, Erizal Zaini, Dwi Setyawan

Article 100320

View PDF Article preview

Responsive nanoparticles in drug delivery systems

Review article *Open access*

Anti-obesity therapeutics through the application of nanostructures in murine models: a systematic review

Rogelio González-Arellanes, Alexandro J. Martagón, Samantha Praget-Bracamontes, Alan V. Olivares-Martínez, Marco Antonio Rito Palomares

Article 100315

View PDF Article preview

Review article *Open access*

Stimuli-responsive nanoparticles in 3D–4D printing for drug delivery: practical considerations and challenges in clinical translation

Isra Dmour, Shorooq Abukhamees, Khawla Dhamen Al-Hamaideh, Eqbal Abu-Alkebash

Article 100318

View PDF Article preview

Previous vol/issue Next vol/issue

About this publication

ISSN: 2352-9520

OpenNano

Open access

17.3
CiteScore

Editorial board

Gender diversity of editors and editorial board members

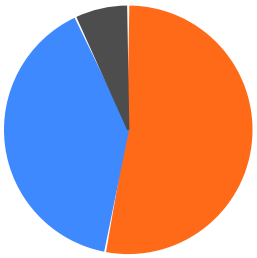

53% woman

40% man

7% prefer not to disclose

0% non-binary or gender diverse

Data represents responses from 78.9% of 19 editors and editorial board members

Editorial board by country/region

19 editors and editorial board members in 13 countries/regions

1 Germany (3)

2 United States (3)

3 Australia (2)

See more editors by country/region

Editor in Chief

Professor Luca Casettari, PhD

University of Urbino, Urbino, Italy

Associate Editor

Professor Jenny Lam, PhD

University College London School of Pharmacy, London, United Kingdom

Nucleic acids, Peptides, Pulmonary drug delivery, Particle engineering, Lipid nanoparticles

View full biography

Editorial Board

Professor Christine Allen, PhD

University of Toronto Leslie Dan, Faculty of Pharmacy, Toronto, Ontario, Canada

Drug delivery, Drug development, Artificial intelligence, Machine learning, Automation, Liposomes and Polymer materials

Professor Mansoor Amiji, PhD

Northeastern University, School of Pharmacy, Department of Pharmaceutical Sciences, Boston, United States

Biomaterials, Pharmaceutical formulations, Nanomedicine, Drug delivery, Gene delivery

View full biography

Prof. Dr. Erem Bilensoy, Prof. Dr.

Hacettepe University, Ankara, Türkiye

Pharmaceutical technology, drug delivery, targeted nanoparticles, 3D printing, nanotechnology, cancer, drug bioavailability, cyclodextrins, oral nanoparticles

View full biography

Assoc. Professor Horacio Cabral

The University of Tokyo, Bunkyo City, Japan

Nanomedicine, Polymeric micelles, Self-assembly, Cancer, Theranostics

Professor Jonghoon Choi, PhD

Chung-Ang University, Dongjak District, Korea, Republic of

Nanomedicine, Nanoparticles, Drug Delivery, Cancer Immunotherapy, Biosensor, Exosomes, Antibacterial

View full biography

Dr. Gregor Fuhrmann, Dr sc ETH

Friedrich-Alexander University Erlangen-Nuremberg, Erlangen, Germany

Infection research, Extracellular vesicles, Biomaterials, Natural products, Biosynthesis

View full biography

Prof. Dr. Olivia Merkel, PhD

LMU Munich, Munich, Germany

RNA formulation, inhalation, dry powder, RNA vaccine, lung disease

View full biography

Professor Dan Peer, PhD

Tel Aviv University The Shmunis School of Biomedicine and Cancer Research, Tel Aviv-Yafo, Israel

Immune-targeted RNA delivery, Systemic, cell-specific delivery of modified mRNA, RNAi as drug-discovery tools in immune cells, Lipid nanoparticle LNP library development and surface functionalization, RNA therapeutics for cancer, Inflammation, and infectious diseases

View full biography

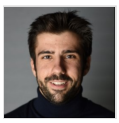

Dr. Quim Peña, PhD

RWTH Aachen University, Aachen, North Rhine-Westphalia, Germany

Nanomedicine, Drug Delivery, Prodrug Chemistry, Metallotherapy, Formulation Chemistry

View full biography

Dr. Hélder A. Santos, PhD

University Medical Centre Groningen, Groningen, Netherlands

Biomaterials for drug delivery, Controlled release systems, Diagnostics, Cancer therapy, Inorganic mesoporous silica/silicon particles, Liposomes and solid lipid nanoparticles

View full biography

Professor Daniela Traini, PhD

Macquarie University, Sydney, New South Wales, Australia

Inhalation Drug Delivery, Aerosols, Dry powders, Pressurised metered dose inhalers, Nebulizer, Inhalatio

View full biography

Honorary Editors

Assoc. Professor Yan Shen, PhD

China Pharmaceutical University School of Pharmacy, Nanjing, China

Pharmaceutics, nanotechnology, in vitro diagnosis, biomaterials

View full biography

All members of the Editorial Board have identified their affiliated institutions or organizations, along with the corresponding country or geographic region. Elsevier remains neutral with regard to any jurisdictional claims.

OpenNano 31 (2026) 100320

Contents lists available at ScienceDirect

OpenNano

journal homepage: www.elsevier.com/locate/onano

Polymer-capped iron oxide nanoparticles: Influence on physicochemical properties and antibacterial efficacy

Karina Citra Rani [a,b], Agnes Nuniek Winantari [b], Tahta Amrillah [c,d], Erizal Zaini [e], Dwi Setyawan [f,g,*]

[a] Doctoral Program in Pharmaceutical Sciences, Faculty of Pharmacy, Universitas Airlangga, Surabaya, 60115, Indonesia
[b] Pharmaceutical Manufacturing Laboratory, Faculty of Pharmacy, University of Surabaya, Surabaya, 60293, Indonesia
[c] Nanotechnology Engineering, Faculty of Advanced Technology and Multidiscipline, Universitas Airlangga, Surabaya, 60115, Indonesia
[d] Airlangga Functional Nanomaterials, Faculty of Advanced Technology and Multidiscipline, Universitas Airlangga, Surabaya, 60115, Indonesia
[e] Department of Pharmaceutics, Faculty of Pharmacy, Universitas Andalas, Padang, 25163, Indonesia
[f] Department of Pharmaceutical Sciences, Faculty of Pharmacy, Universitas Airlangga, Surabaya, 60115, Indonesia
[g] Pharmaceutical Engineering and Processing, Faculty of Pharmacy, Universitas Airlangga, Surabaya, 60115, Indonesia

ARTICLE INFO

Keywords:
Iron oxide nanoparticle
Capping layer
Polymer-capped
Antibacterial efficacy
Infectious diseases

ABSTRACT

Iron oxide nanoparticles (IONP) are versatile materials that exhibit antibacterial properties through membrane damage and ROS production. However, the agglomeration tendency and poor colloidal dispersion in the aqueous medium limit their application. In this study, polymer-capped IONP were developed using three different polymers: polyethylene glycol (PEG 4000), polyvinyl pyrrolidone (PVP K-30), and hydroxypropyl methyl cellulose (HPMC E15) at three different concentrations (0.1%, 0.5%, and 1.0%) to prevent agglomeration and enhance IONP colloidal stability. The successful formation of the polymer-capped IONP was indicated by the hydrogen bond observed from the FT-IR spectrum, interference of the polymer in the crystal lattice of IONP, the smooth surface with an allegedly sheet-like structure, and less agglomerated particles. The application of a capping layer significantly reduced the hydrodynamic particle size of IONP from 140.00±27.90 nm to 82.20±10.14, 68.79±11.50, and 70.07±6.99 nm for IONP capped by PEG 1.0%, PVP 0.1%, and HPMC 1.0%, respectively. The disk diffusion antibacterial assay revealed a higher inhibition zone of the polymer-capped IONP than bare IONP towards *Esherichia coli* and *Staphylococcus aureus*. However, the minimum inhibitory concentration (MIC) determination using the microbroth dilution test possessed limitations in inhibiting bacterial growth due to insufficient direct contact of polymer-capped IONP with the bacterial membrane. The promising polymer-capped IONP systems for further development were IONP-PEG 1.0%, IONP-PVP 0.1%, and IONP-HPMC 1.0%, as depicted through Principal Component Analysis (PCA). The radical scavenging activity presented by polymer-capped IONP enhances its feasibility as an antibacterial agent for infectious diseases and antioxidant properties in the biomedical field.

* Corresponding author at: Department of Pharmaceutical Sciences Faculty of Pharmacy, Universitas Airlangga, Dr. Ir. H. Soekarno Street, Mulyorejo, Surabaya, East Java, Indonesia.
E-mail address: dwisetyawan-90@ff.unair.ac.id (D. Setyawan).

https://doi.org/10.1016/j.onano.2026.100320
Received 5 May 2026; Received in revised form 8 August 2026; Accepted 21 August 2026
Available online 21 August 2026

1. Introduction

Iron oxide nanoparticles (IONP) are ceramic nanoparticles that were employed in the biomedical field as active constituents to overcome specific diseases and promote cellular regeneration. IONP were beneficially incorporated into an injectable hydrogel to stimulate vagus nerve activation and bone remodeling in osteoporosis treatment [1]. From other research, the reactive oxygen species (ROS)-responsive hydrogel containing matrix metalloproteinase-13 siRNA (siMMP-13) and polyethyleneimine (PEI)-polyethylene glycol (PEG) modified Fe_3O_4 nanoparticles was successfully employed as anti-inflammatory and attenuated cartilage degradation [2]. Magnetic IONP was also applicable for antibiotic delivery strategies to overcome prosthetic joint infection through the formation of vancomycin-IONP nanocomposite. The magnetic responsive characteristics of IONP were beneficial to support rapid vancomycin release in the local tissue [3]. Therefore, IONP is a favorable adjuvant and antibacterial agent, particularly for specific site infections.

IONP was a promising antibacterial agent against pathogenic bacteria such as *Staphylococcus aureus, Esherichia coli*, and *Klebsiella pneumoniae*, as reported in an earlier study [4]. Reactive oxygen species (ROS) production via the Fenton reaction was assessed as the primary mechanism underlying its antibacterial activity [5]. ROS interacts with the cell membrane of bacteria, followed by DNA damage and lipid peroxidation, causing cell death [6]. However, the initial study reported that IONP can also exhibit radical scavenging activity characteristics, rather than ROS generation, due to the existence of a capping agent. Therefore, its antibacterial mechanism is not solely determined by ROS generation characteristics but also by physical interaction, electrostatic attraction, and a cell membrane-impairing mechanism leading to cell death. The previous study described that the Fe_2O_3 phase is more pronounced in inhibiting bacterial cell growth compared to the Fe_3O_4 phase, as presented by a lower MIC against *Escherichia coli* [7]. The other study also confirmed that maghemite (γ-Fe_2O_3) exhibited a lower live/dead ratio of *Staphylococcus aureus* compared to magnetite (Fe_3O_4), indicating higher antibacterial activity of this phase [8]. The biomedical application of IONP as an antibacterial compound was limited due to particle agglomeration induced by high surface energy and attraction of magnetic dipole-dipole [6,7]. In addition, the reduction of magnetization capacity and colloidal stability of IONP should also be considered to improve its activity [8,9].

The application of a capping layer is an efficient approach to overcoming these limitations [10–12]. The capping layer is a functional layer composed on the surface of the nanoparticle through covalent and non-covalent interactions, such as hydrogen bonds and van der Waals interactions [13]. The functional group of capping layer materials can attach to the IONP, provoking steric and electrostatic interactions [14]. The steric hindrance and electrostatic repulsion are considered the main mechanisms for preventing IONP agglomeration and improving its physicochemical characteristics [15]. Various materials can be employed as a capping layer, including polymer, surfactant, bio extract, polysaccharide, and amino acids [16]. Polymer is promising for use as a capping layer, as it exhibits both steric and electrostatic stabilization. The polyelectrolyte anchors on the end group of the polymer promote electrostatic repulsion. Meanwhile, the polymer grafting density balances van der Waals interactions among IONP cores through steric hindrance. These mechanisms were reported to be successful in establishing IONP stabilization in colloidal form and minimizing agglomeration [17,18]. Therefore, the physical and chemical properties of the polymer, such as molecular structure, functional group, hydrophilicity, dielectric constant, molecular weight, chain length, and viscosity, must be analyzed to determine a suitable polymer to construct the capping layer [14,15].

The hydrophilic polymer is favorable for modifying the surface of IONP and generating a capping layer. The availability of functional groups, such as -OH, -COOH, -CO, and -NH_2, is beneficial for interacting with the IONP surface [11,16]. The number of functional groups present in the polymer structure determines the probability of interaction and product yield. The polymer functional group also significantly influences the zeta potential and particle size of capped-IONP via electrostatic mechanisms [19,20]. Hence, the adequate zeta potential (> 25 mV) and smaller particle size (< 100 nm) of IONP will be produced by applying a hydrophilic polymer. A hydrophilic polymer that establishes higher viscosity and dielectric constant is recommended as a capping layer, due to its ability to control the nucleation rate and crystal plane growth, resulting in a smaller particle size and better IONP stability [21]. Furthermore, the steric stabilization is implied by the hydrophilic polymer that has a high molecular weight and a longer chain length. The higher molecular weight of the polymer generates a more uniform capping layer and maximum coverage on the surface of the IONP. Additionally, the longer chain length provides better steric stabilization through stronger van der Waals interactions between the polymer and the IONP [22]. However, the molecular weight and chain length of the polymer should be optimized to obtain a desirable capping layer thickness, which significantly impacts the particle size of capped-IONP. Hydrophilic polymers with a molecular weight higher than 1.000.000 Da are not recommended for use as a capping layer, as a previous study reported a significant increase in particle size [22].

In general, a comprehensive study that evaluated the effect of the physicochemical properties of hydrophilic polymers is still limited. The previous work mainly presented the application of a particular polymer to improve the physical and chemical properties of IONP, such as polyethylene glycol [20], polyacrylic acid [23], polyvinyl alcohol [24], Pluronic® P123 [15], and chitosan [25]. Therefore, an elaborate study that investigates the effects of different properties of polymers as a capping layer is still required to select the appropriate polymer. In this study, polyethylene glycol (PEG 4000), polyvinyl pyrrolidone (PVP K-30), and hydroxypropyl methyl cellulose (HPMC E15) are employed as a capping layer in the synthesis of IONP, particularly the maghemite (γ-Fe_2O_3) phase. These polymers have specific functional groups, namely hydroxyl (-OH) in PEG 4000 and HPMC E15, followed by carbonyl (C═O) in PVP K-30. Hence, the hydrogen bond and hydrophobic interaction are predicted to occur between polymers and IONP [14]. These polymers also exhibit extensive polymer chains and high molecular weight, which are 2000–5000 Da, 8000–55.000 Da, and 60.000 Da, for PEG 4000, PVP K-30, and HPMC E-15, respectively [19,23,24]. This characteristic will strongly contribute to the steric stabilization mechanism of IONP. Furthermore, the hydrophilicity and high dielectric constant values of these polymers are also beneficial to maintain nucleation rate and prevent particle agglomeration during synthesis [26–28]. Polymer concentration was also evaluated in this study, since excessive polymer concentration implies zeta potential reduction and particle enlargement [29]. The earlier study

exhibited that the optimal concentration of polymer as a capping layer lies between 0.1 and 1.0%. Consequently, three different concentrations are evaluated for each polymer on the physicochemical properties and antibacterial activity of polymer-capped-IONP, herein 0.1%, 0.5%, and 1.0% [24,26]. We expect this study to emphasize the effect of polymer properties on the physicochemical and antibacterial efficacy of polymer-capped IONP, in conjunction with determining the potential polymers to improve IONP's characteristics and biomedical applications.

2. Materials and methods

2.1. Materials

The materials used in this study include chemical reagents (analytical grade) and pharmaceutical excipients (pharmaceutical grade). The chemical reagents consist of ferric chloride hexahydrate 98% ($FeCl_3{\cdot}6H_2O$) (Sigma-Aldrich) and sodium hydroxide (NaOH) pellets (Merck). The pharmaceutical excipients employed in this study are polyethylene glycol (PEG 4000) (NOF Corporation, Japan), polyvinylpyrrolidone (PVP K-30) (JH Nanhang Life Sciences, China), and hydroxypropyl methyl cellulose (HPMC E15) (Shanghai Honest Chem Co., LTD, China). Double-distilled water (PT. Ikapharmindo, Indonesia) was used in all the synthesis procedures. Hypoxanthine (Sigma-Aldrich), xanthine oxidase (Sigma-Aldrich), and nitroblue tetrazolium chloride (NBT) (Thermo Fisher, Merck) reagents were employed for ROS scavenging activity analysis.
The Mueller-Hinton agar medium (Merck) and the bacteria isolated (*E. coli* ATCC 8739 and *S. aureus* ATCC 6538) obtained from the Indonesian National Agency of Drug and Food Control (Badan POM Indonesia) were utilized for the antibacterial efficacy test of these polymer-capped IONP. The bacterial strains were stored on agar slants at 4 °C and subsequently cultured in nutrient broth at 37 °C for 24 h. The disk diffusion method was performed in this study to evaluate the antibacterial efficacy of polymer-capped IONP using Thermo Scientific™ Oxoid™ blank antimicrobial susceptibility discs. Muller-Hinton broth medium (Merck) was employed for minimum inhibitory concentration (MIC) determination.

2.2. Synthesis of iron oxide nanoparticles (IONP)

The IONP samples were synthesized using the previously optimized co-precipitation method [30]. We used the precursor concentration of 0.10 M and 2 M sodium hydroxide solution, with the stirring process conducted at 600 rpm, as these parameters could generate excellent physicochemical properties of the synthesized IONP [31]. The stirring process continued for 3 h. The reddish-brown precipitate was separated from the supernatant by centrifugation at 4000 rpm for 10 min [32]. Afterwards, the precipitate was washed using double-distilled water until a neutral pH was achieved (pH =7), indicating the removal of excess ions, particularly the chloride ions. The drying process of these precipitates is then conducted in an oven at 80 °C for 24 h [33]. The post-precipitation thermal treatment and annealing process was not conducted in the synthesis process of IONP to prevent phase conversion from the favorable maghemite (γ-Fe_2O_3) phase to the more stable α-Fe_2O_3 (hematite) phase, since α-Fe_2O_3 (hematite) produced lower magnetization and antibacterial activity [34].

2.3. Synthesis of polymer-capped iron oxide nanoparticles (IONP)

The prepared IONP was coated using three different types of hydrophilic polymer, namely PEG 4000, PVP K-30, and HPMC E15. Each polymer was optimized in three concentrations of the capping layer: 0.1%, 0.5%, and 1.0%. IONP powder was weighed at 300 mg, then dispersed in 50 mL of double-distilled water. The polymer solution was then prepared by dissolving a specific amount of polymer in 50 mL of double-distilled water, thereby obtaining the desired concentration in a 100 mL mixture. The polymer solution was added dropwise using a syringe into the IONP dispersion, while stirring at 600 rpm with a magnetic stirrer at room temperature (25–30 °C) [35]. The stirring process then continued for 6 h under these conditions until a light reddish-brown suspension was formed. Subsequently, the suspension was centrifuged at 4000 rpm for 10 min to settle the polymer-capped IONP precipitate, and a magnetic separation process was conducted. The precipitate was then washed thoroughly using 100 mL of double-distilled water to remove the excess polymer [36]. The precipitate was then dried in an oven at 60 °C for 12 h [37]. The dried powder of polymer-capped IONP was stored in an airtight container for further evaluation.

2.4. Characterization of polymer-capped iron oxide nanoparticles (IONP)

The interaction between IONP and the polymers as a capping layer was investigated through a Fourier-transform infrared (FT-IR) spectrophotometer (Jasco 4200 type A) [20]. The powder X-ray diffraction (PXRD) pattern of the polymer-capped IONP was recorded using a Rigaku MiniFlex 600-C Powder X-ray Diffractometer to analyze the surface functionalization of the polymer [14]. The UV–Vis spectrum and optical properties of polymer-capped IONP were analyzed using a UV–Vis spectrophotometer (Shimadzu UV-1800) at a wavelength of 200–800 nm. The band gap energy calculation was also performed from the obtained UV–Vis spectrum data [38]. The morphological state, microstructure, size, and chemical composition of the polymer-capped IONP were studied using a Thermo Scientific Phenom ProX scanning electron microscope equipped with an energy-dispersive X-ray detector (SEM-EDX). The particle size was also determined from the SEM micrograph at 10,000× magnification by measuring 100 particles using ImageJ software [39]. The chemical constituents and distribution of these constituents that comprise the polymer-capped IONP were also detected by an Energy Dispersive X-ray (EDX) detector equipped with the SEM instrument [40]. The

hydrodynamic particle size and surface charge of polymer-capped IONP were determined using a Malvern Zetasizer Pro Advance (Malvern Instruments, UK) equipped with a dynamic light scattering module [25]. The magnetic properties analysis of the polymer-capped IONP was carried out using a vibrating sample magnetometer (VSM) at room temperature (300 K) using a magnetic field up to 30 kOe [36]. The statistical analysis of particle size and zeta potential was performed using the Kruskal-Wallis Test at the 0.05 significance level (α=0.05). The software for statistical analysis was IBM® SPSS Statistics 23 (IBM Corporation).

2.5. *In vitro antibacterial activity study of polymer-capped iron oxide nanoparticles (IONP) using disk diffusion method*

The disk diffusion method was used to assess the antibacterial efficacy of polymer-capped IONP prepared using PEG 4000, PVP K-30, and HPMC E15. The antibacterial efficacy of these polymer-capped IONPs was evaluated against *Escherichia coli* (ATCC 8739), a gram-negative bacterium, and *Staphylococcus aureus* (ATCC 6538), a gram-positive bacterium [6]. These bacteria were subcultured in nutrient broth for 24 h before use. The turbidity of the bacterial suspension was adjusted to 0.5 McFarland (approximately $1–2 \times 10^8$ CFU/mL). Approximately 60 µl of bacterial suspension was spread on the surface of an agar plate. The samples were prepared by dissolving each polymer-capped IONP in methanol until a final concentration of 1000 µg/ml was reached. The filter paper disk was impregnated with this solution, then transferred to a nutrient agar plate. Methanol as a solvent was employed as a negative control; meanwhile, amoxicillin was prepared as the positive control. The neodymium magnet (OMOT8ESV) with a 5 mm diameter was put on the surface of the Petri dish to modulate the magnetization properties of polymer-capped IONP for enhancing its antibacterial properties. The inhibition zone diameter (mm) was measured using a vernier caliper for each sample and was conducted in three replicates [41].

2.6. *Principal component analysis (PCA) of physicochemical properties and antibacterial activity of polymer-capped iron oxide nanoparticles (IONP)*

Principal component analysis (PCA) technique was employed to analyze the multivariate relationship between physicochemical properties and antibacterial activity of polymer-capped iron oxide nanoparticles (IONP). PCA simplified the data into a lower-dimensional space, derived from the principal components (PC), which were combinations of the original variables, and explained the maximum variability of these variables [42]. The polymer-capped IONP dataset includes hydrodynamic particle size, polydispersity index (PDI), zeta potential, SEM-derived particle size, band gap energy, magnetization, and inhibition zone diameter against *Staphylococcus aureus* and *Escherichia coli*. Principal component analysis (PCA) was conducted on the correlation matrix using eigenvalue decomposition, and components with eigenvalues > 1.0 were further applied for analysis. Afterwards, the scree plot, loading plot, and score plots were generated to evaluate variance distribution, variable contributions, and clustering map of each polymer-capped IONP formulation [43]. All the analysis processes were performed using Minitab® Statistical Software 22. The most promising systems of each polymer-capped IONP were further analyzed.

2.7. *Transmission electron microscopy (TEM) characterization*

The morphological characteristics of the most promising systems for each type of polymer-capped IONP, determined by PCA analysis, were further examined using a transmission electron microscope (TEM, JEOL JEM-1400). The core size of IONP was determined by measuring the diameter of 50 randomly selected particles, and then the particle size distribution and average particle size were analyzed using ImageJ software [44].

2.8. *Reactive oxygen species (ROS) scavenging activity analysis*

The behavior of polymer-capped IONP for generating or scavenging ROS was studied using nitro blue tetrazolium (NBT), since NBT can directly react with the produced ROS, particularly superoxide anion radical ($O_2^{\bullet -}$), to form a purple-blue formazan precipitate. The preliminary study of polymer-capped IONP exhibited ROS scavenging activity rather than generating. Hence, the ROS scavenging activity was performed by a series of polymer-capped IONP solutions with concentrations of 5000, 2500, 1250, 625, and 312.5 ppm. Hypoxanthine and xanthine oxidase solutions were employed to generate ROS and as a negative control. Each concentration of polymer-capped IONP and NBT reagent (20:2 ratio) was added to the hypoxanthine-xanthine oxidase solution. The samples were incubated for 30 min at a temperature of 37° C, and the absorbance was analyzed using a microplate reader (Biochrom EZ Read) at a 560 nm wavelength [45].

2.9. *2.9 Minimum inhibitory concentration (MIC) and minimum bactericidal concentration (MBC) determination*

The selected system of polymer-capped IONP, according to the PCA analysis, was further studied regarding its antibacterial activity profiles. MIC determination was performed by the broth microdilution method using 96-well titer plates. The stock solution of polymer-capped IONP (10.000 ppm) was prepared by dispersing the samples in 5 ml double distilled water. Afterward, the test solution was prepared ranging from 5000, 2500, 1250, 625, and 312.5 ppm using Mueller-Hinton Broth (MHB) as dilution. Approximately 100 µL of test solutions were put in the wells. The bacterial culture (*Escherichia coli* and *Staphylococcus aureus*) was prepared to a 0.5 McFarland standard inoculum, then diluted to 1:100 using MHB and added to each well. The positive control containing bacterial inoculum in MHB and the negative control, consisting of MHB only, were also prepared. The plates were incubated for 24 h at a

temperature of 37 °C. The optical density (OD) of *Escherichia coli* was measured at 600 nm wavelength, while *Staphylococcus aureus* was measured at 595 nm, followed by the determination of MIC. After determining the MIC values, 100 ul of the samples from transparent wells were put on Mueller-Hinton Agar (MHA) for culturing and incubated at 37 °C for 24 h. The MBC was determined by the lowest concentration of polymer-capped IONP that successfully killed the bacteria [46].

3. Results and discussion

3.1. Fourier transform infrared (FT-IR) spectroscopy analysis

The interaction between IONP and the polymer matrix, which serves as a capping layer, was studied using FT-IR spectroscopy. The absorption band of IONP and polymer-capped IONP was analyzed to determine the possible interaction formed during the synthesis [47]. The FT-IR spectra and peak assignments of IONP and IONP capped by PEG 4000, PVP K-30, and HPMC E15 are displayed in Fig. 1, **Supplementary Fig. S1, and Supplementary Table S8**. The bare IONP presented the bonds due to O—H stretching at 3433.87 cm^{-1} and O—H bending at 1626.13 cm^{-1}. These bonds are probably due to the absorbed water on the surface of the IONP [34]. The previous study also revealed that the absorption band around 1623.90 cm^{-1} is correlated with the vibration mode of γ-Fe_2O_3 and can be further confirmed by the PXRD patterns analysis [48]. The specific absorption was observed at 590.65 cm^{-1} and 878.06 cm^{-1} indicating the Fe-O stretching of Fe_2O_3. Moreover, the absorption band at 590.65 cm^{-1} was specifically displayed for maghemite (γ-Fe_2O_3), which was previously reported between 590 cm^{-1} and 634 cm^{-1} [49]. Hence, the phase of the prepared IONP was predicted as maghemite (γ-Fe_2O_3).

The FT-IR spectrum of all polymer-capped IONPs exhibited small absorption around 2350–2360 cm^{-1}. This peak presumably confirmed the existence of environmental CO_2 absorption during FT-IR spectroscopy analysis [32]. The application of PEG 4000 as a capping layer on the prepared IONP provoked the absorption band around 1100 cm^{-1}, due to the C—O-C stretching that is typically associated with PEG ether linkage. The shift of C—O stretching from 1104.35 cm^{-1} in the PEG spectrum to ~ 1000–1016 cm^{-1} in IONP-PEG systems suggested the hydrogen bonding between the oxygen ether (C—O) of PEG and IONP. The -OH group of PEG as a capping layer was also implied to intensify the -OH stretching vibration around 3430–3450 cm^{-1}, since PEG was an ethylene glycol derivative [14]. Thus, the hydrogen-bound interaction between PEG and the surface of IONP is presumably a dipole-cation bound between the ether group of PEG and the positive charges of IONP [20]. In addition, the increment of PEG concentration as a capping layer exhibited a more intense absorption of -OH stretching (3430–3450 cm^{-1}) and C—O-C stretching, preserving the stronger interaction between PEG 4000 and IONP. The enhancement of this absorption implied both polymerization of the PEG chain on the surface of IONP and hydrophilicity improvement of the capped-IONP [50].

The FT-IR spectrum of PVP-capped IONP exhibited characteristic peaks of IONP, including Fe-O stretching at 668 cm^{-1}, -OH stretching at 3446–3450 cm^{-1}, and -OH bending from water adsorption molecules at 1639–1646 cm^{-1}. The peak shifting of the amide carbonyl group (C═O) of PVP from 1655.19 cm^{-1} to 1639–1646 cm^{-1} indicated the interaction between PVP and the IONP core. The presence of PVP in the capping layer was observed to intensify the absorption band around 1639–1646 cm^{-1} due to the existence of the carbonyl group (C═O) from PVP that interacted with the IONP, promoting surface functionalization. The interaction that was constructed on the PVP-capped IONP might be due to the oxygen on the carbonyl (C═O) group of PVP and the proton contained in the maghemite (γ-Fe_2O_3) [14]. Meanwhile, the peak at 894.51 cm^{-1} was assigned to the vibration of the pyrrolidine ring of PVP, indicating the pyrrolidine ring attachment on the prepared PVP-capped IONP, as reported before around 880 cm^{-1} [51]. The increase in PVP K-30

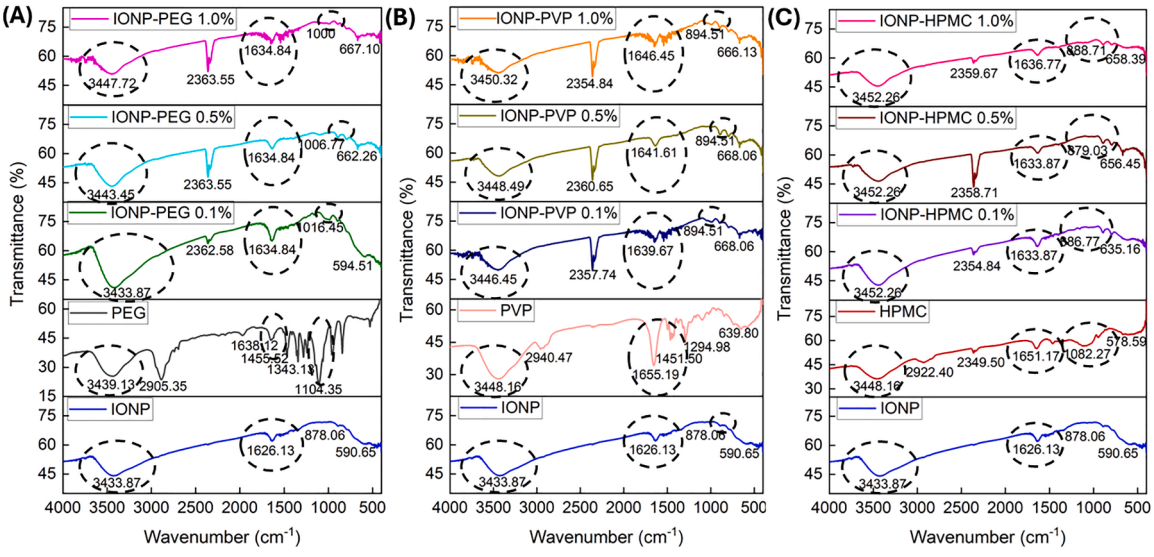

Fig. 1. The FT-IR spectrum of (A) IONP-PEG capped systems, (B) IONP-PVP capped systems, and (C) IONP-HPMC capped systems.

concentration applied as a capping layer induced the broadening of the -OH stretching band, which indicated the thicker capping layer attached to the surface of IONPs, constructed from hydrogen bonding. However, the thickening of the capping layer formed on the surface of IONP could reduce the strength of the coordination interaction between the Fe^{3+} ion and PVP. Therefore, the appropriate concentration of PVP as a capping layer must be investigated for the physicochemical properties of IONP [25,43].

The existence of HPMC molecules as a capping layer on the surface of IONP was confirmed by the broad FTIR band at 3452.26 cm^{-1}, which indicated -OH stretching from the HPMC functional group. The transmission band is also located at 3600–3100 cm^{-1}, which is particularly maximum at 3461 cm^{-1} and correlated with the -OH groups of HPMC molecules. Since the pure HPMC molecules exhibited specific bending vibrations around 1650 cm^{-1} due to water molecules' vibration, the shifting to 1633.87–1636.77 cm^{-1} correlated with hydrogen bonding formation between the hydroxyl group of the HPMC side chain and Fe-O [38,44]. The C—O-C stretching of HPMC shifted from 1082.27 cm^{-1} to 879.03–888.71 cm^{-1}, indicating interaction between glycosidic parts of cellulose derivatives like HPMC with IONP [52]. Meanwhile, the Fe-O vibrational modes are still detected at 635.16–658.39 cm^{-1}. These results showed the successful surface functionalization of HPMC without altering the IONP core. Increasing the HPMC concentration as a capping layer from 0.1% to 0.5% caused the broadening of the -OH stretching bond around 3452 cm^{-1}. On the contrary, the intensity of these peaks appeared lower in IONP-HPMC 1.0%, indicating reduced surface coverage as HPMC concentrations increased and produced a high-viscosity dispersion. This was presumably due to the separation of the HPMC viscous layer during the synthesis process. The FT-IR spectrum of all polymer-capped IONP exhibits specific interactions between the functional group of the polymer and IONP, remarking the successful capping layer coverage on the surface of IONP [37].

3.2. X-ray diffraction (XRD) analysis

XRD patterns of IONP and polymer-capped IONP prepared from this study are presented in **Supplementary Fig. S2**. The broader peak and low intensity from the IONP diffraction pattern suggested the formation of a nanocrystalline sample [53]. A small diffraction peak associated with the ɣ-Fe_2O_3 phase, which could be located at $2\theta = 35.50^{\circ}$, was observed in all the polymer-capped IONP samples [54]. The existence of the γ-Fe_2O_3 phase confirmed that the capping layer did not alter the IONP core structure and phase. γ-Fe_2O_3 phase is preferable due to its ability to produce superparamagnetic properties, high saturation magnetization, and higher antibacterial activity reflected from the lower minimum inhibitory concentration (MIC) values compared to the other phase [7]. However, the application of a capping layer influenced the peak breadth and intensity, presumably due to the reduction in crystallite size and surface disorder [14].

The application of PEG, PVP, and HPMC as a capping layer is attributed to the presence of a typical polycrystalline phase on the

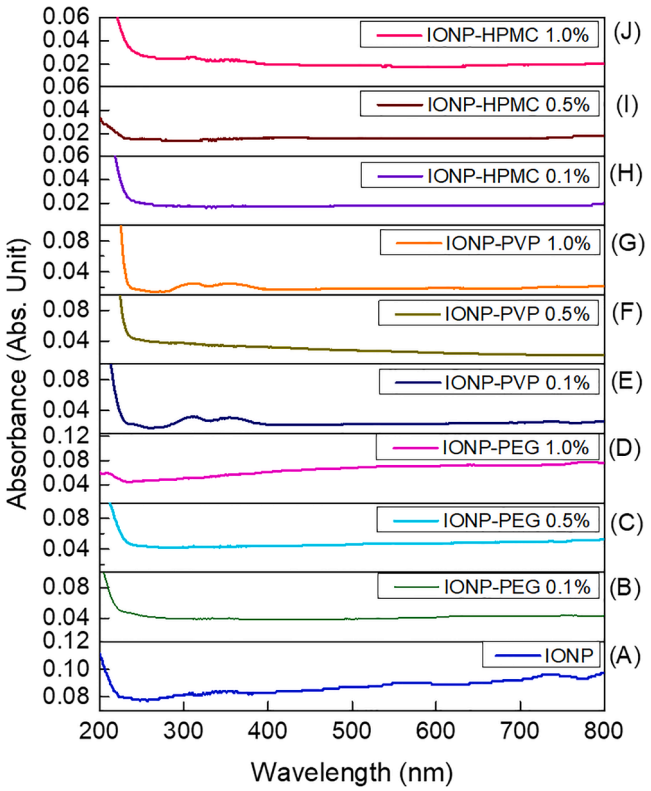

Fig. 2. UV–Vis spectrum of (A) IONP, (B) IONP-PEG 0.1%, (C) IONP-PEG 0.5%, (D) IONP-PEG 1.0%, (E) IONP-PVP 0.1%, (F) IONP-PVP 0.5%, (G) IONP-PVP 1.0%, (H) IONP-HPMC 0.1%, (I) IONP-HPMC 0.5%, (J) IONP-HPMC 1.0%.

surface of the IONP, especially at 2θ values of ~15 °- 25 ° The reduction of XRD peak intensity was also observed due to the existence of the capping layer on the surfaces of IONPs [37]. PEG is a hydrophilic polymer with the lowest molecular weight and viscosity among the polymers investigated [20]. Hence, PEG formed a flexible, low-viscosity chain layer around the surface of IONP without significantly altering its crystal structure. Moreover, PVP exhibited a thicker capping layer due to its higher molecular weight and vigorous coordination via the carbonyl groups of the pyrrolidone ring [51]. This condition led to a more crystalline reduction and a higher defect density. Additionally, HPMC, which presented the highest molecular weight and viscosity, produced a thicker capping layer and an amorphous shell [55]. The thicker capping layer pronounced peak broadening, elevated micro strain, and reduced grain size, which was extensively presented by the application of 1.0% HPMC [56]. The peak broadening and reduction of peak intensity were also intensified as the capping layer increased from 0.1% to 1.0%. Therefore, increasing the concentration of polymer as a capping layer significantly reduced the crystallinity of IONP [20]. Nevertheless, the reduction in crystallinity of IONP does not always have a negative impact. Some active sites on the surface of IONP could arise from this phenomenon, further enhancing the antibacterial activity of the IONPs [56,57]. We discuss this effect in detail in the antibacterial activity assessment.

3.3. UV–Vis spectrum and band gap energy analysis

UV–Vis spectra of IONP and polymer-capped IONP samples are carried out to evaluate their optoelectronic properties, which are displayed in Fig.2. This evaluation is important to determine the surface state of the samples, which further correlates to their antibacterial performance. The unmodified IONP showed broad shoulders at 321 nm, confirming the successful formation of IONP. The absorbance peaks at around 272–321 nm indicate the formation of IONP due to a direct transition, specifically a ligand-metal charge transfer transition (Fe-O transition) [4]. The other absorbance, presented between 420–600 nm, was also reported as a local crystal field transition and pair excitation [58]. In this study, the IONP displayed this absorbance at 556 nm. The absorbance that was presented in this visible region (400–800 nm) also correlated with the brick red color, which caused absorption in this region [4]. The polymer-capped IONP, using PEG, PVP, and HPMC, presented a similar profile of the UV–Vis spectrum to the unmodified IONP. However, the absorbance of unmodified IONP was higher compared to the polymer-capped IONP. The UV–Vis spectrum of polymer-capped IONP exhibited alteration of peak intensity, width, and shape, although the main absorption, which presented Fe-O stretching, was still observed clearly. This alteration was presumably due to surface chemistry modification, improved dispersion, and refractive index modification. Thus, the application of polymer as a capping layer did not significantly change the core of IONP conformation, implying that the modification of the capping layer only modified the surface of IONP [25].

The broadening absorbance that indicated Fe-O stretching was pointed out by the UV–Vis spectrum of polymer-capped IONP. This change was remarkably related to the surface modification of the polymer, which influenced the passivation of the Fe-O surface sites and the reduction of aggregation [25]. The lower absorbance of the specific peak around 380–420 nm was presented in the polymer-capped IONP spectrum because of the presence of the polymer. The polymer, as a capping layer attached to the surface of IONP, then increased the molecular mass and steric stabilization, resulting in the reduction of aggregation tendency. The quantum size effect of the polymer as a capping layer was attributed to the blue shift in the wavelength of polymer-capped IONP, since these polymers preserved particle size reduction and better colloidal dispersion [38]. The previous study also indicated that the observed blue shift (hypsochromic shift) of maximum absorption was related to the particle size reduction, which corresponds to higher energy absorption [24].

The application of a PEG capping layer induced the Fe-O absorption shifting from 315 nm to 305 nm, due to surface defect transitions and colloidal dispersion. The increase in PEG concentration as a capping layer was also reported to intensify the blue-shifting phenomenon and surface plasma resonance (SPR) broadening, as well as a reduction of absorbance value due to a thicker capping layer [59]. The flatter visible long-wavelength spectrum of PEG-capped IONP was presented from the IONP capped by higher PEG concentration (0.5% and 1.0%), resulting from the reduction of light scattering. The thicker PEG capping layer provoked higher steric hindrance, leading to minimal particle-particle interaction and preventing particle agglomeration [60]. The capability of this capping layer to prevent agglomeration and clumping, as captured in the UV–Vis spectrum, was considered by the individual nanoparticles rather than the light scattering due to agglomerated particles [61].

The identical properties of peak broadening, blue shifting, and reduced specific absorption were also observed in the IONPs-capped PVP layer. However, PVP capping influenced a higher tendency of surface defects due to the modification, which implied the appearance of a shoulder band around 300–360 nm and a smoother spectrum [62]. The broad and flatter spectrum is also characterized in the visible region, since PVP modulated stronger effects on the surface of IONP through carbonyl group coordination. Through this interaction, PVP was able to provide stronger steric stabilization and decrease the particle size, which is considered the primary factor of blue shifting and narrow extinction bands [51]. The larger extent of the blue shift and the decline of visible region absorption were produced along with the increase of PVP as a capping layer. Thus, the surface coverage and steric hindrance capacity can be reported as highly correlated to the amount of PVP molecules, which is studied by varying PVP concentrations.

Meanwhile, HPMC, which exists as a bulkier structure and has a higher molecular weight, constructed a thicker hydrophilic layer on the surface of IONP. Noticeable blue shifting and a smoother spectrum in both UV and visible regions were presented in the HPMC-capped IONP spectrum. This phenomenon was gradually observed as the HPMC concentrations increased from 0.1% to 0.5%. These results indicated that the higher viscosity of the HPMC capping layer determined the higher steric hindrance and presumably smaller size of IONP [52]. Nevertheless, the higher amount of HPMC molecules at the 1.0% concentration presented the opposite condition. The higher absorbance in the UV region and the rugged visible absorption were observed. This might be due to the phase separation of the viscous film layer of HPMC during synthesis, implicating weaker surface coverage and incomplete polymer coating on the IONP [27].

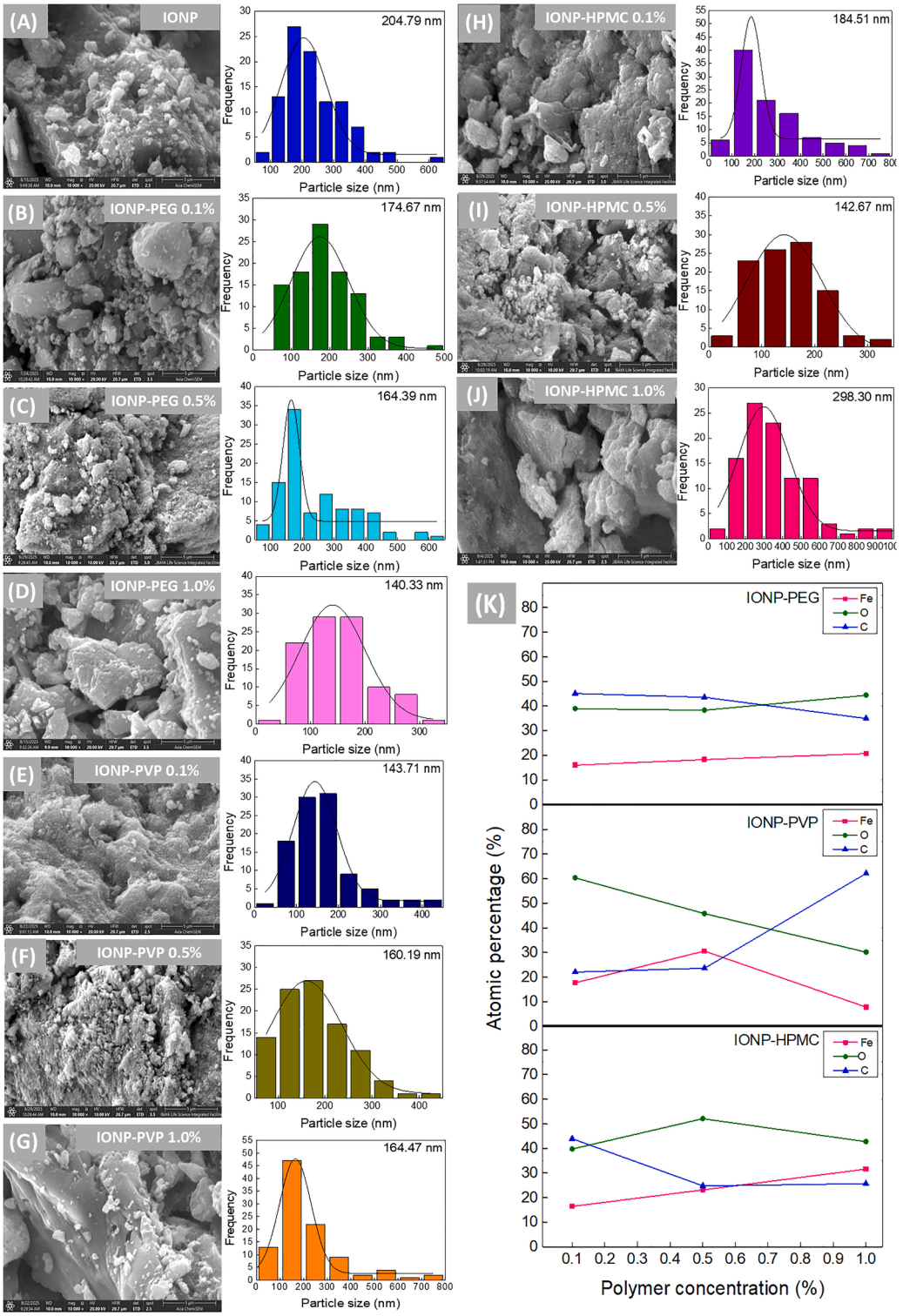

Fig. 3. SEM Micrograph (10,000x magnification) and particle size distribution calculated using Image J software (n = 100): (A) IONP, (B) IONP-PEG 0.1%, (C) IONP-PEG 0.5%, (D) IONP-PEG 1.0%, (E) IONP-PVP 0.1%, (F) IONP-PVP 0.5%, (G) IONP-PVP 1.0%, (H) IONP-HPMC 0.1%, (I) IONP-HPMC 0.5%, (J) IONP-HPMC 1.0%, and (K) Atomic percentage of Fe, O, and C for each Polymer-capped IONP system.

The band gap energy of polymer-capped IONP can be determined using the Tauc equation and presented in the **Supplementary Fig. S3.** The band gap energy of the prepared IONP from this study was 1.80 eV. The application of polymer as a capping layer, herein PEG, PVP, and HPMC, exhibited an increment in the band gap energy value. The PEG-capped IONP presented a band gap energy between 2.05 and 2.11 eV; furthermore, the PVP-capped IONP and HPMC-capped IONP showed band gap energies around 2.42–2.94 eV and 2.36–2.63 eV, respectively. The enhancement of the band gap energy through the application of a polymer capping layer consequently resulted from the reduction of particle size and the quantum confinement effect [38]. The increase in band gap energy marked the escalation of the energy gap between the valence and conduction bands [62]. This information gives an important hint about the role of the polymer capping layer in the properties of IONPs, which further affect their application as an antibacterial agent.

3.4. Morphology, particle size determination, and elemental mapping analysis using SEM- EDX

Scanning Electron Microscopy (SEM) analysis was carried out in this study to evaluate the morphology of IONP and polymer-capped IONP by three different polymers (PEG, PVP, and HPMC). The particle size and distribution were also determined from the SEM micrograph using ImageJ by measuring 100 particles. The SEM micrograph of IONP and polymer-capped IONP, equipped with the particle size distribution curve and atomic percentage of Fe, O, and C atoms from each system, is presented in Fig. 3. The morphology of the uncapped IONP was a nearly spherical particle with a rough surface; additionally, the aggregation of IONP particles was detected. The aggregation tendency of uncoated IONP was due to the Van der Waals force and dipole-dipole interaction between magnetic particles [39]. The aggregation of uncoated IONP was also confirmed from the particle size determination, since this IONP exhibited a higher average particle size (204.79 nm) and a broader particle size distribution curve, rather than the polymer-capped IONP.

The application of a capping layer was reported to modify the morphology of IONP slightly, particularly at lower (0.1%) and moderate (0.5%) concentrations of the capping layer. The more spherical shape and smooth surface are constructed from these polymer-capped IONPs. The smoother surface of polymer-capped IONPs was observed upon the increase in polymer concentration. These results are in accordance with the study performed by Hussein et al., which reported that the amount of surface coating agent significantly influences morphology and surface roughness [37]. More homogeneously distributed IONP clusters were also presented from the SEM images of polymer-capped IONP, indicating the capability of the capping layer to enclose the surface of IONP and produce an adequately monodispersed system [22]. However, the sheet-like structure and irregular morphology of polymer-capped IONP at 1.0% polymer concentration were observed. The excessive amount of capping agent was probably considered to be the cause of this result. In line with this finding, the morphology of capped-IONP that was prepared by citric acid, sodium dodecyl sulfate, and polyvinyl alcohol as a capping layer was also significantly controlled by the capping agent molar concentration [37].

The effect of polymer concentration was necessary to control the particle size distribution of IONP. PEG, as the lowest molecular weight polymer employed in this study, had a significant impact on the particle size reduction along with the escalation of this polymer concentration. IONP capped by PEG 1.0% provoked a narrower particle size distribution and the smallest particle size, compared to the uncapped IONP and the other concentrations. This was presumably due to the higher steric efficiency of 1.0% concentration of PEG, which hindered particle-particle interaction that promoted agglomeration [20]. On the contrary, the larger particle size was obtained as the PVP concentration in the capping layer increased. Lower molecular weight and PVP concentration were more favorable for spreading out regularly on the nanoparticles' surface because of the high number of single chains available for this purpose. When increasing the amount of PVP, the polymer-polymer interaction is more prominent than the polymer-IONP interaction. Hence, a more complex polymer assembly was established, prompting particle size enlargement [63]. HPMC demonstrated a distinguished profile of particle size reduction as a capping layer. The increment of HPMC concentration from 0.1% to 0.5% was beneficial for reducing particle size from 184.51 nm to 142.67 nm. However, the application of 1.0% HPMC resulted in the formation of a larger particle size due to entrapment in a sheet-like assembly. The excessive polymer concentration and thicker film-like properties of HPMC were pointed out as the considered factor for this significant augmentation of particle size [55]. The larger particle size determined by the SEM-derived method was caused by the self-assembly of nuclei entrapped in the micelle structure of the polymer matrix [33]. These results are probably different compared to the hydrodynamic particle determination using dynamic light scattering (DLS), because the DLS method captured the size of particles under Brownian motion in the specific medium [64]. Thus, the particle size of polymer-capped IONP measured from the SEM images must be compared to the colloidal state measurement, such as using DLS.

The atomic percentage of atoms that compose polymer-capped IONP is presented in Fig. 3(K), and the energy dispersive X-ray (EDX) spectrum of polymer-capped IONP is depicted in the **Supplementary Fig. S4**. The EDX spectrum of IONP consisted of Fe and O atoms, with atomic percentages of 40.3% and 59.7%, respectively. The atomic percentages of the prepared IONP in this study confirmed the formation of the Fe_2O_3 phase, since the stoichiometric ratio between iron (Fe) and oxygen (O) is close to 0.66 [65]. The EDX spectrum of the polymer-capped IONP showed Fe and O peaks, indicating that the Fe_2O_3 phase remained in the samples. Whereas the apparent peaks of C and O can be attributed to the polymer capping layer, herein, PEG, PVP, and HPMC. From these results, the capability of the polymer as a capping layer was established by enveloping the IONP core on its surface [66]. The application of PEG as a capping layer significantly enhanced the C peaks signal, while the Fe attenuation typically drops from 40.3% in the bare IONP to 16.0% after capping by PEG. PEG highly assigned C and O signals due to its (-CH_2—CH_2—O) backbone, maintaining the continuity of the shell structure across the IONP core. The O signal remained constant because both PEG and IONP contained O. However, as the PEG concentration increased, the atomic percentage of the C atom gradually decreased due to the viscoelastic properties of the PEG solution, which are concentration-dependent. The higher PEG concentration formed a more viscous and higher shear modulus of the PEG solution, which created a boundary layer between the surface of the IONP and the bulk solution [67]. Thus, the lower adsorption efficiency was notable as the decline of the atomic percentage of the C atom, implicating the reduction of the PEG layer thickness.

In general, the EDX spectrum of PVP-capped IONP revealed that the thickness of the PVP capping layer was highly influenced by the increment of PVP concentrations. As PVP concentrations increased from 0.1% to 1.0%, the atomic concentration of the C atom increased. The application of 0.1% PVP resulted in a light adsorption capping layer, characterized by a slight increase in C atomic

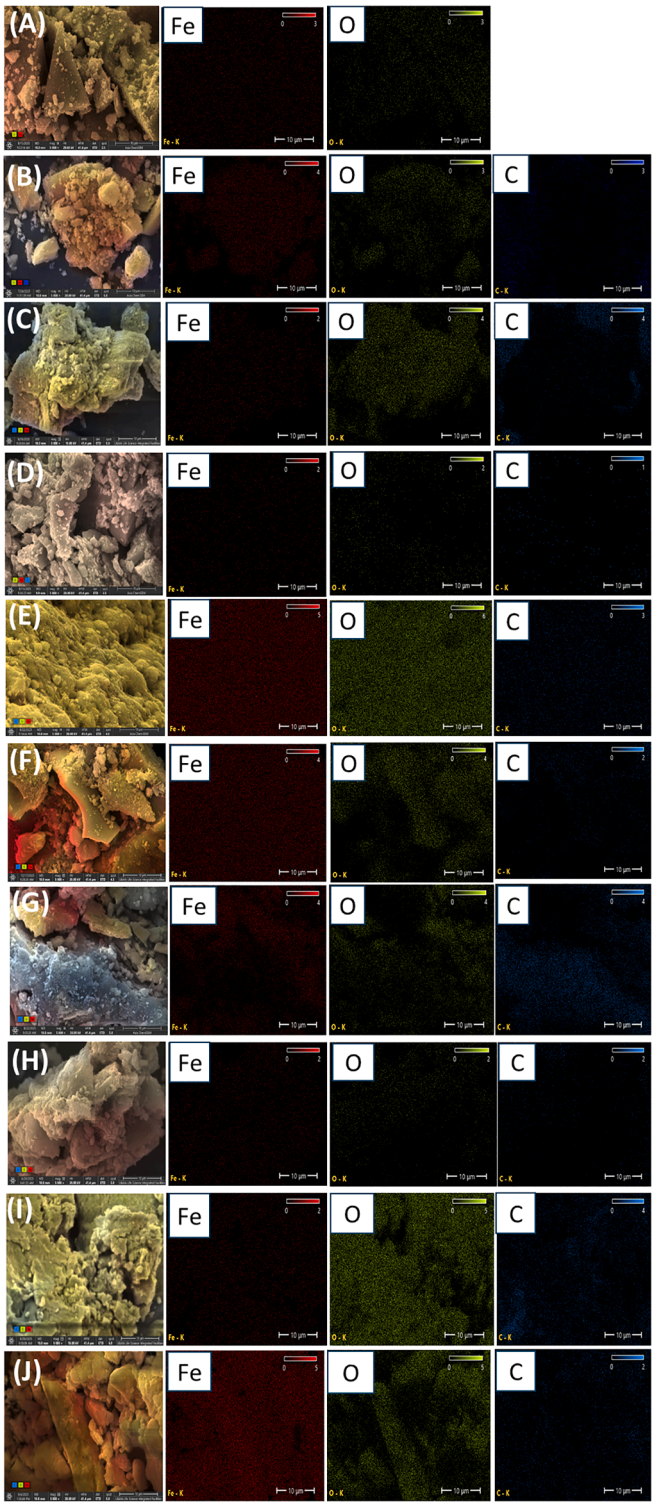

Fig. 4. Elemental mapping at 5000x magnification of (A) IONP, (B) IONP-PEG 0.1%, (C) IONP-PEG 0.5%, (D) IONP-PEG 1.0%, (E) IONP-PVP 0.1%, (F) IONP-PVP 0.5%, (G) IONP-PVP 1.0%, (H) IONP-HPMC 0.1%, (I) IONP-HPMC 0.5%, (J) IONP-HPMC 1.0%.

concentration and partial reduction of Fe concentration compared to the uncapped IONP. The thick PVP capping layer was observed on the IONP capped with 1.0% PVP, as indicated by the strong C signal and the highest atomic concentration of C atoms, followed by a suppressed Fe concentration. It was also noted from the previous study that a higher PVP concentration resulted in a thicker capping layer and unselective adsorption on the surface of IONP because of stronger interactions on the surface of IONP and polymer agglomeration [51]. The surface roughness captured from the SEM images was suspected of influencing the inhomogeneous distribution of the PVP capping layer [68]. The HPMC-capped IONP also indicated the effect of polymer concentration on the capping layer formation. The reduction of surface coverage homogeneity by the higher concentration of HPMC was presented through a gradual reduction of the C atomic concentration and the advancement of Fe atomic concentration. The 0.1% capped IONP sample by HPMC was exposed as the polymer-rich region, but the higher concentration presented a more core-exposed region. It can be predicted that owing to particle clustering, coalescence, and aggregation at higher concentrations of HPMC influencing the discontinuous polymer

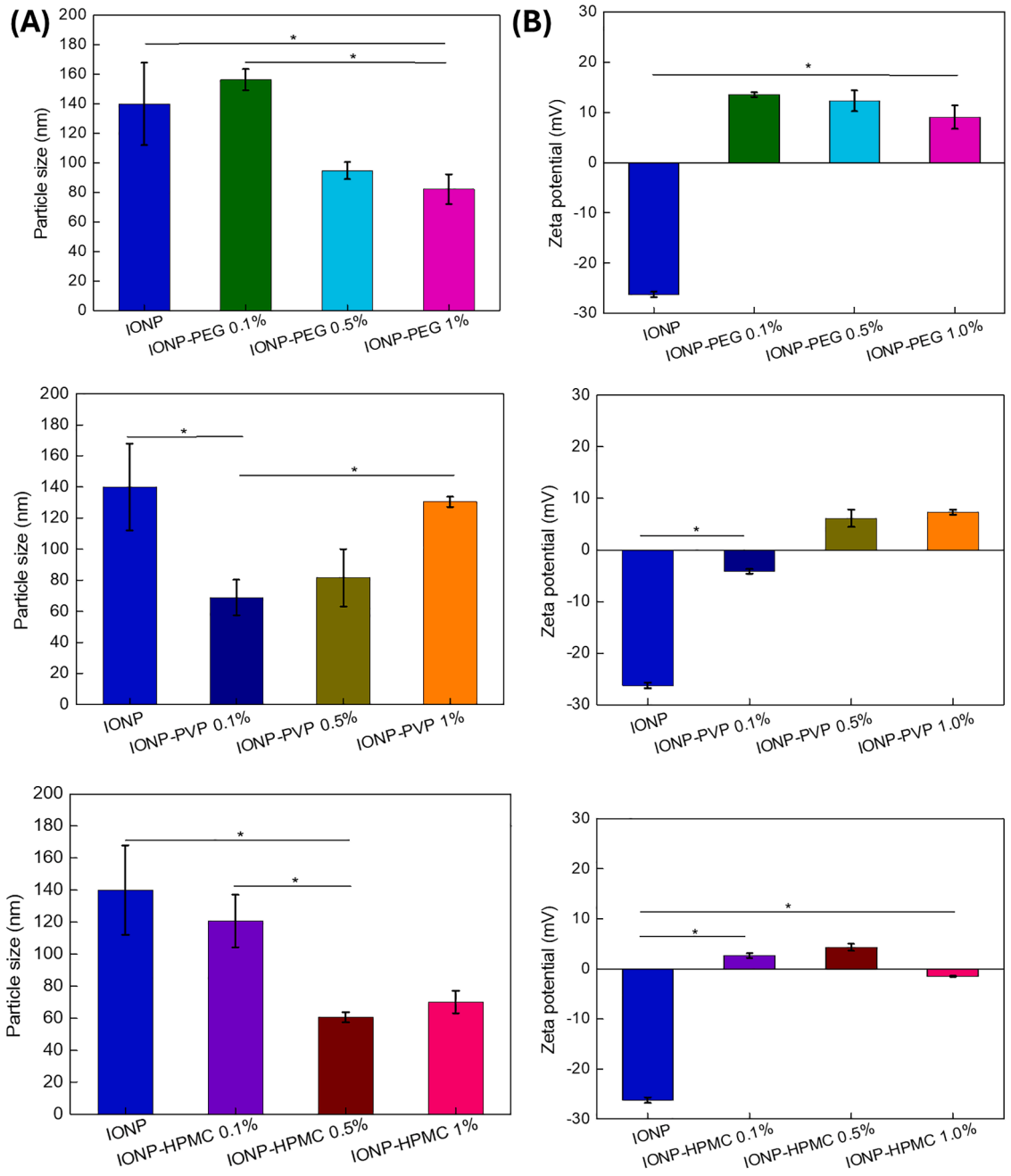

Fig. 5. (A) Hydrodynamic particle size (Z-average) of polymer-capped IONP and (B) Zeta potential of polymer-capped IONP. Results are calculated as mean ± standard deviation (SD) from three replicates (n = 3).

coverage [69].

The distribution of the chemical components of IONP and polymer-capped IONP is presented in Fig. 4. The elemental mapping exhibited that IONP was structurally composed of Fe and O atoms, indicated by the red and lime green colors, presenting the purity of the Fe_2O_3 phase [4]. The presence of the C domain and intense O color in the polymer-capped IONP, either for PEG, PVP, or HPMC, revealed the successful capping of IONP with these polymers. The sharp yellow color observed from the surface of the majority of the polymer-capped IONP suggested that the system was oxygen-dominant [70]. Moreover, carbon (C) is also an essential element that builds the PEG, PVP, and HPMC molecular structure; hence, the presence of this component on the surface of polymer-capped IONP reflected the adhesion of these polymers on IONP [71]. The PEG-capped IONP showed a homogeneous distribution of the capping layer in the three concentrations applied, as recorded by the scattered blue color indicating C elements. However, the irregular and discrete distribution of the capping layer was presented by PVP-capped IONP at 1.0% concentration due to the high viscosity of the PVP solution. The EDX spectrum and mapping elements of HPMC-capped IONP presented the uniform distribution of the capping layer on the surface of IONP, depicted by the C atoms scattered regularly. The intense red color from the IONP capped by HPMC 1.0% revealed the reduction of capping layer thickness in the high polymer concentration. The viscosity and critical shear rate of the polymer were determined by polymer concentration. In a concentrated polymer solution, polymer entanglement was observed, and the non-Newtonian behavior also contributed to the limitation of polymer distribution. For the non-Newtonian solution, the shear rate of the system was lower at a higher concentration upon the application of a similar shearing stress. This phenomenon reduced the diffusivity on the surface of the solid material; therefore, the thickness of the capping layer was reduced [72].

3.5. 3.5 Hydrodynamic particle size and zeta potential analysis

The principal determination of the hydrodynamic particle size was due to the Brownian motion of the particles that diffuse within the dispersion fluid. Thus, these data represented the indication of particle agglomeration [73]. The dispersion behavior of IONP and polymer-capped IONP in double-distilled water is presented in **Supplementary Fig. S5**. Meanwhile, the hydrodynamic particle size of IONP and polymer-capped IONP was depicted in Fig. 5(A). The uncoated IONP exhibited a hydrodynamic particle size (Z-average particle size) of 140±27.89 nm, generally larger than the polymer-capped IONP prepared in this study. For PEG-capped IONP, the application of 0.1% and 0.5% PEG concentration did not significantly reduce the particle size of IONP ($p > 0.05$). Meanwhile, the increase in PEG concentration to 1.0% was beneficial in reducing the particle size of PEG-capped IONP compared to the uncoated IONP ($p < 0.05$). The lower polydispersity index (PDI) value of PEG-capped IONP (PDI = 0.17–0.32) suggested a narrower particle distribution and more uniform particle size after the application of the capping layer than the uncoated IONP (PDI = 0.58). The higher steric hindrance produced by the higher concentrations of PEG was predicted as the predominant factor that controlled the particle size, although the thinner capping layer was constructed, as discussed from the SEM-EDX results. As more molecules of PEG were attached to the surface of IONP in the primary layer, a higher surface area/volume ratio was exhibited, which led to particle growth inhibition by the established capping layer. The DLVO theory also outlined that the capped colloidal particles produced minimum aggregation due to particle repulsion influenced by the steric hindrance [60].

The smaller particle size and more uniform distribution were also presented by PVP-capped IONP than the uncoated IONP, as presented by the PDI value, which is between 0.26 and 0.51. However, the application of PVP as a capping layer revealed a different trend compared to PEG, since the increment of PVP concentration caused hydrodynamic particle size enlargement. IONP capped by PVP at 1.0% concentration showed the highest particle size, and the resulting particle size was not significantly different compared to the IONP ($p > 0.05$). Otherwise, the capping layer that was constructed by PVP 0.1% was particularly favorable to reduce the IONP particle size significantly to 68.79±11.50 nm compared to the uncoated IONP and IONP capped by 1.0% PVP ($p < 0.05$). The presence of high PVP concentrations affected the capping layer construction on the surface of IONP. The first layer was formed by the initial PVP molecules adsorbed on the surface, followed by the other parts that dissolved in the reaction medium to form the capping layer [74]. At higher PVP concentrations, the distribution of the first layer was not uniform, and the thickness of the capping layer was concentrated in a specified region. The EDX spectrum analysis also confirmed that the thickness of the PVP capping layer increased, particularly at 1.0% polymer concentration. Nevertheless, the elemental mapping profile shown in Fig. 4 indicated that the capping layer was not homogeneously dispersed. The thickness of the capping layer and the inhomogeneous distribution of the capping layer that induced IONP agglomeration probably determined the particle size enlargement at higher PVP concentration applied [75].

On the other hand, the application of HPMC 0.1% as a capping layer was pointed out not to have significantly influenced the particle size reduction of IONP. Whereas IONP capped by HPMC 0.5% exhibited a smaller particle size than the uncoated IONP, as well as the HPMC-capped IONP at 0.1% concentration ($p < 0.05$). This substantial reduction of particle size was presumably due to the enhanced agglomeration hindrance and stabilization by applying a higher concentration of capping layer on the IONP surface. A higher concentration of HPMC as a capping layer formed multi-layer adsorption on the surface of IONP, providing more steric hindrance and electrostatic repulsion. Consequently, these mechanisms resisted IONP aggregation in the dispersion medium [76]. The hydrodynamic size profile for each polymer-capped IONP was in accordance with the previous particle size determination from the SEM images, indicating an adequate correlation between these particle size evaluation methods to predict the impact of polymer concentrations as a capping layer.

The zeta potential value of uncoated IONP and polymer-capped IONP was determined by the Zetasizer instrument, as presented in Fig. 5(B). Zeta potential indicated the potential difference between the sliding plane of the electrical double layer adsorbed on the surface of particles and the bulk medium [65]. The surface charge of IONP and polymer-capped IONP samples can be estimated by zeta potential value determination [77]. Since the colloidal stability of IONP was determined by both the steric and electrostatic repulsion, the evaluation of zeta potential needs to be conducted. Nanoparticles that employed zeta potential values greater than +25 mV or less

than –25 mV preserved high colloidal stability [78]. Considering the interaction between the polymer-capped IONP interface and bacteria, the surface potential of the prepared IONP also plays a vital role in the attachment process and ROS production [79]. The zeta potential value of the uncoated IONP was found to be −26.26±0.55 mV, indicating sufficient colloidal stability in aqueous medium. The negative zeta potential value of IONP was correlated with the negative charge of the hydroxyl group due to water adsorption on the surface of IONP, which maintained its stability [31,69]. When PEG was applied as a capping layer on the surface of uncoated IONP, the zeta potential charge was inversely converted from a negative to a positive value. The positive value of the PEG-capped IONP was similar to Hayashi et al result, which indicates slightly positive values close to zero in the neutral aqueous medium [80]. The zeta potential value of the PEG-capped IONP prepared in this study ranged from 9.05±2.35 to 13.53±0.44 mV. The immobilized PEG layer on the surface of the IONP altered the zeta potential value due to its surface coverage properties and the existence of functional groups from the polymers. PEG exhibited a non-ionic character, and the hydroxyl group is only at the end of the polymer structure. Therefore, the effect of surface charge was minimized, attributed to the conversion to the positive charge, and decreased the zeta potential value [80].

PVP as a capping layer at 0.1% concentration also significantly reduced the zeta potential value of IONP ($p < 0.05$), followed by the alteration of the zeta potential charge into a positive value when a higher concentration of PVP was applied. The lower zeta potential value of PVP-capped IONP compared to the PEG capping layer indicated the higher surface coverage capacity of PVP due to longer chain length, higher molecular weight, and more intense interaction, particularly by carbonyl and amino groups. Furthermore, the thickness of the PVP-capping layer, along with the increase in PVP concentration, resulted in a slight escalation of the zeta potential value. This was presumably due to more ions adsorbed on the surface of IONP upon the application of an abundant PVP concentration [44]. The addition of an HPMC layer to the surface of IONP was reported to strongly shield the existing surface charge of uncoated IONP until close to zero values. The masking effect of HPMC correlated with its complex structure and higher molecular weight, primarily compared to PEG and PVP. The previous study explained that the electric neutrality properties of HPMC are considered in reducing the electrostatic repulsion of mineral particles. According to the results, the long carbon chain of HPMC was considered the main factor in reducing the zeta potential value of HPMC-capped IONP [81].

Although the zeta potential value of all the polymer-capped IONP in this study was lower than |25| mV, indicating a poor electrostatic stabilization mechanism, the utilization of these polymers was still beneficial to produce steric stabilization. The steric stabilization mechanism occurred from the osmotic force, which is established when the polymeric shells of aggregates overlap [82].

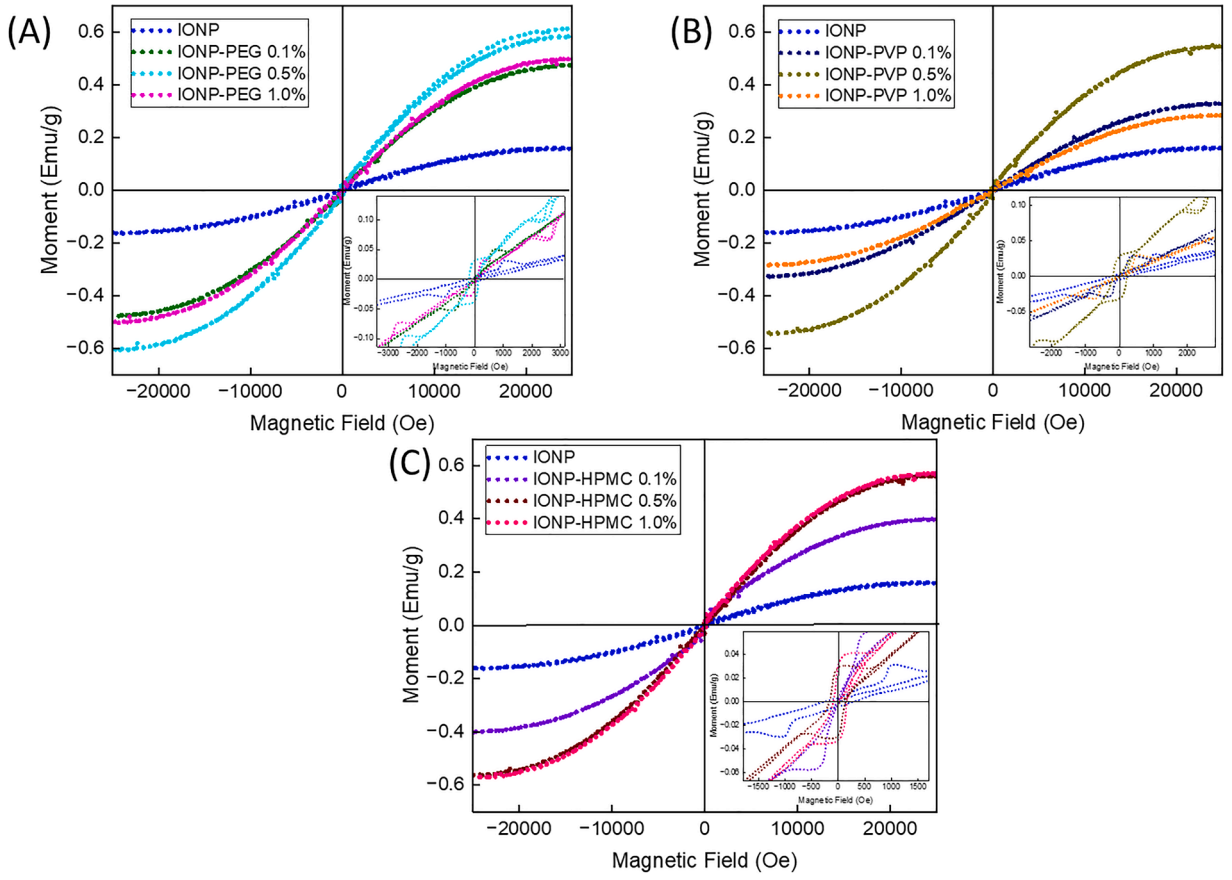

Fig. 6. Magnetic properties (M-H hysteresis curve) of polymer-capped IONP (A) IONP-PEG, (B) IONP-PVP, and (C) IONP-HPMC.

Thus, this force repels the Van der Waals interaction between particles and thus prevents direct particle contact [28]. In addition, during the nanoparticle synthesis, the specific group of the polymer chain attaches to the forming nanoparticle, while the loose polymer chain constructs an adsorption layer on the surface [63]. The controlled particle size of IONP and nearly monodisperse particle size distribution of polymer-capped IONP obtained from this study indicated that the steric stabilization of this polymer was sufficient to improve the colloidal stability of IONP [83].

3.6. Magnetization characteristics of IONP

The magnetization characteristics of IONP and all polymer-capped IONP were examined using a vibrating sample magnetometer (VSM) at room temperature, as depicted in Fig. 6. The sigmoidal (S-shaped) magnetization curve associated with a low saturation magnetization (Ms) response was observed when the external magnetic field was applied to the uncoated IONP. The magnetization curve of uncoated IONP also exhibited remanent magnetization (Mr) and coercivity (Hc) close to zero. From these characteristics, uncoated IONP can be categorized as superparamagnetic materials. Superparamagnetic materials contain several unpaired electrons that exhibit an electronic moment or spin [84]. The unpaired electron spins align along the direction of the external magnetic field, presented as a magnetic moment. When the external magnetic field is absent, a zero average magnetic moment is characterized by the superparamagnetic materials [85]. The magnetization characteristics of the uncoated IONP were different from the bulk maghemite (γ-Fe_2O_3), which exhibited ferrimagnetic character at room temperature [86].

The magnetization curve of polymer-capped IONP prepared in this study exhibited nearly S-shaped M-H loops, which are typically characterized as superparamagnetic materials. The negligible remanent magnetization (Mr) and coercivity (Hc) also suggested the superparamagnetic behavior of all the samples. The PEG-capped-IONP that was prepared by Tai et al. showed similar trends, wherein the reduction of particle size contributed to the reduction of Mr and Hc values [64]. The superparamagnetic behavior of the polymer-capped IONP suggested its benefits for biomedical applications like drug delivery and magnetic hyperthermia, due to its field-dependent moment in the magnetic field and low tendency to form agglomerates in physiological media [87]. The magnetization curves of the polymer-capped IONP revealed distinct variations in M_S, Mr, and H_C as presented in Table 1, driven by both polymer type and concentration. In general, the application of PEG, PVP, and HPMC as a capping layer improved the magnetization characteristics of IONP. The application of a polymer, categorized as an organic coating layer, altered the surface spin structure, making it more regular and aligned in the same direction. Moreover, the capping layer also contributed to decreasing particle anisotropy due to the bonds between the polymer and surface cations of IONP, resulting in an improvement of magnetic properties. Several factors were reported to affect these properties, such as the functional group of the polymer, the length of the chain, the electronic structure, and the strength of the bond between IONP and polymer [88]. The loops from the magnetization curve presented very small hysteresis compared to the uncoated IONP, suggesting the excellent performance of the capping layer to suppress the Hc and Mr values, probably due to fewer agglomerates and better dispersion characteristics of these polymer-capped IONP.

A similar M_S enhancement pattern was observed in the IONP capped by PEG and HPMC. When the polymer concentration increased from 0.1% to 0.5%, the magnetization value increased gradually. This confirmed the favorable surface atom interaction and the promising effect of particle size reduction on the surface spin arrangement [89]. Kaaragac and Kockar also reported the same results: as the PEG amount increased from 5 to 25 *g*, the saturation magnetization (Ms) of the polymer-capped IONP gradually increased, starting from 52.3 to 58.5 emu/g. The existence of a capping layer also contributed to preventing particle agglomeration and maintaining the superparamagnetic properties [36]. However, the application of a 1.0% concentration of those polymers revealed slightly magnetic suppression compared to the prepared IONP with a 0.5% capping layer. The thicker insulation capping layer or strong steric stabilization probably influenced this phenomenon. The diamagnetic shell produced by the capping layer was considered to reduce the magnetization [17,42]. Meanwhile, PVP exhibited a greater reduction in magnetization at the same loading (1.0%) than PEG and HPMC. The magnetization value of PVP-capped IONP at 1.0% concentration was remarkably decreased below that of the IONP capped by 0.1% concentration. This phenomenon presumably occurs due to the tighter binding and more compact shells, in line with the SEM-EDX result (Fig. 3) that revealed the thicker capping layer established by PVP at this concentration. The existence of a non-magnetic outer shell, composed of higher concentrations of PVP, influenced spin disorder in the core-shell structure, further decreasing the magnetization [44].

Table 1
Saturation magnetization (Ms), remanent magnetization (Mr), and coercivity of IONP and polymer-capped IONP.

System	Saturation magnetization (Ms) (emu/g)	Remanent magnetization (Mr) (emu/g)	Coercivity (Hc) (Oersted)
IONP	0.1632	0.0029	190.88
IONP-PEG 0.1%	0.4734	0.0021	44.41
IONP-PEG 0.5%	0.5950	0.0349	160.99
IONP-PEG 1.0%	0.4995	0.0008	68.55
IONP-PVP 0.1%	0.3264	0.0002	44.24
IONP-PVP 0.5%	0.5431	0.0287	189.54
IONP-PVP 1.0%	0.2829	0.0012	39.52
IONP-HPMC 0.1%	0.4013	0.0016	24.74
IONP-HPMC 0.5%	0.5590	0.0288	160.39
IONP-HPMC 1.0%	0.5774	0.0311	92.56

3.7. In vitro antibacterial activity analysis by disk diffusion method

IONP is a versatile material that exhibits antibacterial activity through membrane damage mechanisms, reactive oxygen species (ROS) generation, DNA damage, lipid peroxidation, and mitochondrial disruption [90]. Several interactions, including hydrogen bonds, Van der Waals forces, electrostatic forces, and hydrophobic interactions, were considered in the attachment of IONPs to the bacterial cell membrane. However, these interactions were reported to be randomly established between the IONP and the surface cell membrane, resulting in different responses to each bacterial strain [91]. Despite the bacterial strain, the properties of the prepared IONP and the culture conditions also influenced the antibacterial response of IONP toward the bacterial cell [92]. Therefore, in this study, two different antibacterial strains, which represent the Gram-positive and Gram-negative bacteria, were employed to evaluate the antibacterial activity of polymer-capped IONP, namely *Staphylococcus aureus* and *Escherichia coli*, respectively. The membrane of Gram-positive bacteria, such as *Staphylococcus aureus,* consists of a compact peptidoglycan layer and teichoic acid. On the contrary, Gram-negative bacteria like *Esherichia coli* exhibit a thin peptidoglycan layer, followed by outer lipopolysaccharide membranes [93]. The antibacterial activity of IONP and polymer-capped IONP was studied using these bacterial strains by the Kirby-Bauer disk diffusion method. The results of inhibition zone diameter measurements are explained in Fig. 7. The observation of inhibition zone diameter towards *Staphylococcus aureus* and *Escherichia coli* was presented in **Supplementary Figs. S6 and S7**.

The prepared IONP and polymer-capped IONP were observed to be more susceptible to *Staphylococcus aureus*, which is included as a Gram-positive bacterium, than *Escherichia coli*, which is known as a Gram-negative bacterium, since a higher diameter inhibition zone was produced. The higher interaction of IONP with *Staphylococcus aureus* cells was considered the main factor that exhibited a higher antibacterial activity compared to *Escherichia coli* [94]. Similar results were also presented by a polymer-capped IONP that was prepared with PEG, PVP, and HPMC as a capping layer. However, the greater inhibition zone diameter was ascertained from the majority of polymer-capped IONP preparations compared to the bare IONP for both bacterial strains. The smaller particle size and more uniform distribution of polymer-capped IONP particles were presumably considered to enhance the antibacterial activity [95]. The smaller particle size of nanoparticles led to stronger interactions on the active sites (-SH) of the protein cell membrane and better penetration through this membrane, followed by the release of oxidative stress to the intracellular level [5].

In addition, the alteration of zeta potential charge from a negative value for uncoated IONP to a positive value for polymer-capped IONP was also beneficial to enhance the surface interaction, since the surface charge of bacteria was generally negative. However, the higher adsorption saturation density was employed by the Gram-negative bacteria, approximately seven-fold higher than that of the Gram-positive bacteria, suggesting that a higher concentration of positively charged molecules is required to saturate the exterior surface [96]. Thus, at the same concentration of exposure, the amount of IONP molecules diffused and generated antibacterial action was limited in the Gram-negative bacteria, as depicted by the lower inhibition zone diameter observed. The magnetic properties of polymer-capped IONP also contributed to the improvement of the antibacterial activity of this system for targeted transport in the bacterial cell. The lower concentration of IONP with superparamagnetic properties, as pointed out in this study, was reported to be effective in inhibiting bacterial cell growth and minimizing its toxicity on human cells [97].

The antibacterial activity profile of polymer-capped IONP prepared in this study was reported to be highly influenced by the type of polymer as a capping layer and its concentration. For PEG-capped IONP, the increased PEG concentration, as a capping layer, is generally followed by an increment in the inhibition zone diameter for both bacteria, *Staphylococcus aureus* and *Escherichia coli*. The significant reduction in particle size and better polydispersity index were predicted to be the main factors that contributed to the

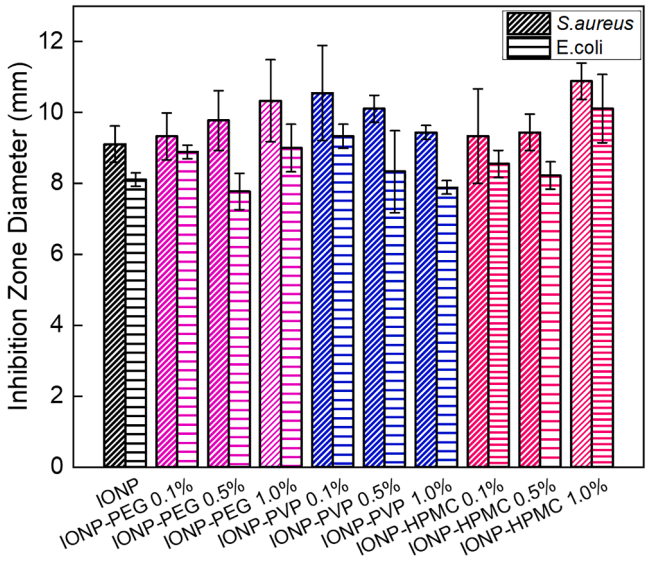

Fig. 7. Inhibition zone diameter of IONP, IONP-PEG, IONP-PVP, and IONP-HPMC towards *Staphylococcus aureus* and *E. coli*. Results were calculated from three replicates (n = 3) and presented as mean ± SD.

higher inhibition capacity of these IONPs. The smaller particle size of IONP results in a higher surface area to volume ratio, which enhances free energy content and reactivity. These properties are substantially correlated with their capability to diffuse and permeate the cytoplasmic region of the bacterial cell membrane [98]. Additionally, the escalation of the atomic percentage of Fe depicted from the EDX spectrum was also considered to be a prominent factor that enhanced the ROS production. The occurrence of PEG as a capping layer can inhibit particle aggregation and improve the electrostatic adsorption of the IONP due to the positive charge of the IONP surface after capping by PEG molecules. These properties were beneficial to induce oxidative stress reactions and ROS production, in conjunction with membrane cell disruption and cell breakdown, which led to bacterial cell death [77].

The effect of particle size on the antibacterial activity of the polymer-capped IONP was also established for PVP-capped IONP samples. Since the escalation of PVP concentrations significantly enhanced particle size enlargement of the PVP-capped IONP, the lowest PVP concentration as a capping layer was preferable to produce smaller, more homogeneous IONP particles. Therefore, the IONP prepared by PVP as a capping layer at 0.1% concentration was promising as a potential system to overcome both *Staphylococcus aureus* and *Escherichia coli* due to its higher antibacterial inhibition capacity. Although the surface charge of the IONP-PVP 0.1% system was negative, it produced a greater inhibition of bacterial growth. The main mechanism that improved its antibacterial activity was presumably due to the particle size effect, despite the surface charge interaction mechanism. The particle size controlled the bio-distribution, physical penetration, and Fe ion release towards bacterial cell membranes [99]. The smaller IONP particle size and nanocrystalline properties exhibited a higher surface area to volume ratio, which enabled greater penetration of smaller IONP and active sites enhancement, leading to internal damage and disruption of bacterial metabolic processes [100].

Similar patterns regarding the effect of particle size of capped-IONP on the antibacterial activity were observed from the HPMC-capped IONP. The higher inhibition zone diameter for both bacterial strains was observed with IONP as the concentration of HPMC in the capping layer increased. IONP capped with HPMC as a capping layer in 1.0% concentration exhibited higher antibacterial activity due to the smaller particle size and a larger band gap energy, implicating the higher intracellular ROS production through greater availability of excitons [101]. The higher antibacterial activity of HPMC-capped IONP was also observed towards *Staphylococcus aureus* than *Escherichia coli* across all capping layer concentrations. Gram-positive bacteria are composed mainly of a thick peptidoglycan layer and lack a protective barrier, enabling a more accessible penetration process and antibacterial exertion mechanism [102]. The closely spherical morphology, sheet-like structure, and more edges of the HPMC-capped IONP prepared by a 1.0% capping layer were

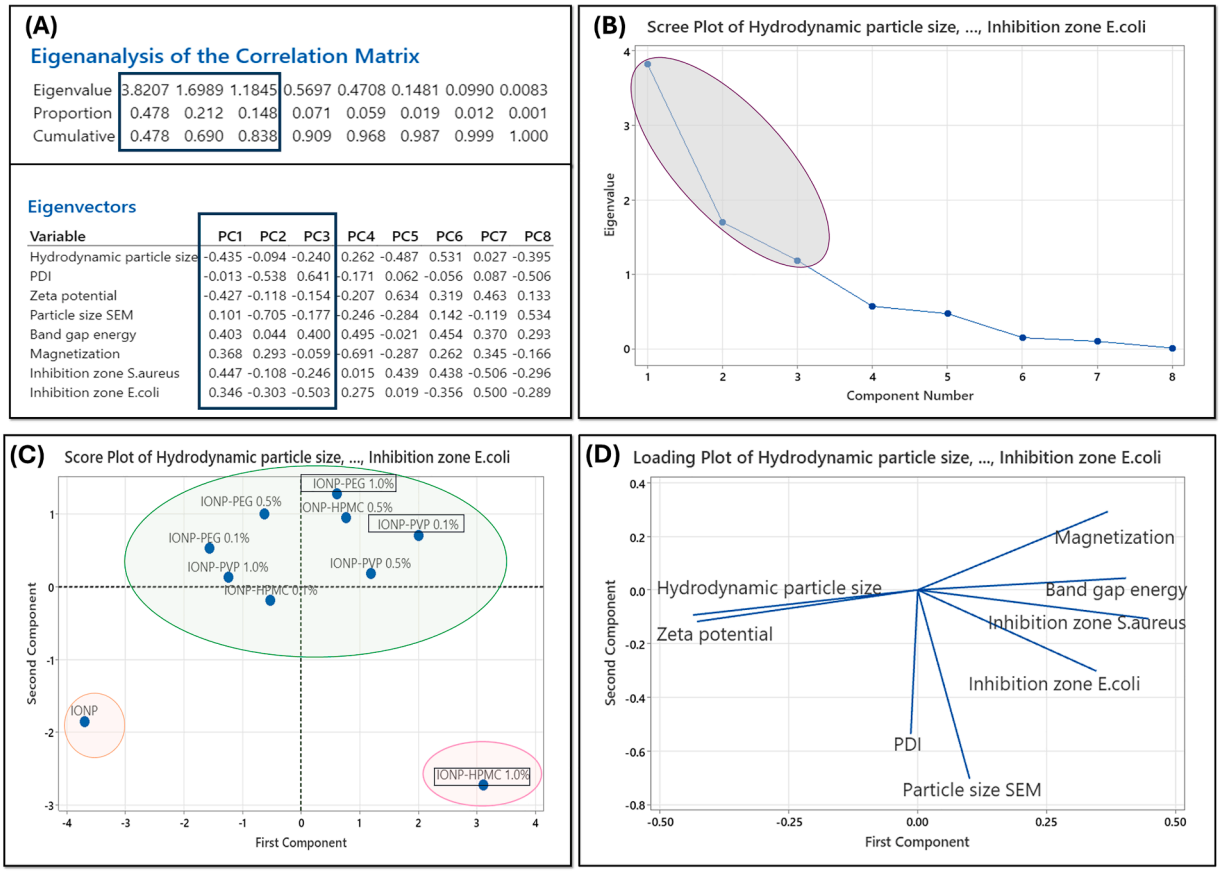

Fig. 8. The result of principal component analysis (PCA): (A) Eigenanalysis of the correlation matrix and eigenvector values, (B) Scree plot, (C) Score plot, and (D) Loading plot.

predicted to be highly related to the efficient contact of this nanoparticle with the bacterial cell membrane [103]. The gradual increase in Fe atomic percentage with HPMC concentration was also considered a necessary factor in ascertaining the enhancement of antibacterial activity. Since the stabilization mechanism of IONP capped by HPMC was predominantly through steric effect, the efficient capping process and uniform dispersion of IONP were achieved in the higher HPMC concentration (1.0%) [104]. Based on the antibacterial activity test, the application of PEG, PVP, and HPMC as capping layers was favorable for improving the antibacterial activity of IONP.

3.8. Principal component analysis (PCA) of polymer-capped IONP physicochemical properties and antibacterial activity

Principal component analysis (PCA) was reported to be applicable in reducing the dimensionality of the dataset of physicochemical properties and antibacterial activity of polymer-capped IONP synthesized in this study. PCA, as a powerful data exploration tool, was prominent for data categorization and comparability [43]. The results of the eigenanalysis of the correlation matrix, the scree plot, score plot, and loading plot are depicted in Fig. 8. The eigenanalysis results and scree plot revealed that the three principal components (PC1, PC2, and PC3) were considered the main contributing factors due to the cumulative ratio contributed by these factors lying at 0.838 (83.8%) of the total variance. Additionally, the eigenvalue of these factors was > 1.0, indicating a significant contribution [105]. Therefore, these factors were sufficient to capture the dominant patterns in physicochemical properties and antibacterial activity.

Principal component 1 (PC1) contributed 47.8% of the variance in the data and was the most influential component in this model [43]. PC1 is primarily derived from hydrodynamic particle size, zeta potential, band gap energy, and inhibition zone against *Staphylococcus aureus* and *Escherichia coli*. However, the principal component 2 (PC2) contributed to 0.212 (21.2%) of the data variance. PC2 was dominated by the polydispersity index (PDI), SEM-derived particle size, and magnetization. The homogeneity of particle size and magnetic properties of these polymer-capped IONP was presented from this component as essential parameters that affected the nanoparticle performance and surface interactions with bacterial membranes. In addition, the principal component 3 (PC3) revealed a contribution at 0.148 (14.8%) to the variance. This component dominantly highlighted the polydispersity index (PDI), band gap energy, and inhibition zone diameter, which reflected the antibacterial activity of these polymer-capped IONP. The scree plot also indicated that PC1, PC2, and PC3 were the main components that influenced the data variance, since the shoulder plot and eigenvalue > 1 were constructed by these components, as depicted in Fig. 8(A) and 8(B).

The score plot (Fig. 8C) and loading plots (Fig. 8D) captured the clustering tendency of polymer-capped IONP based on their physicochemical and antibacterial properties due to the polymer type and concentrations. The bare IONP separated as a distinct

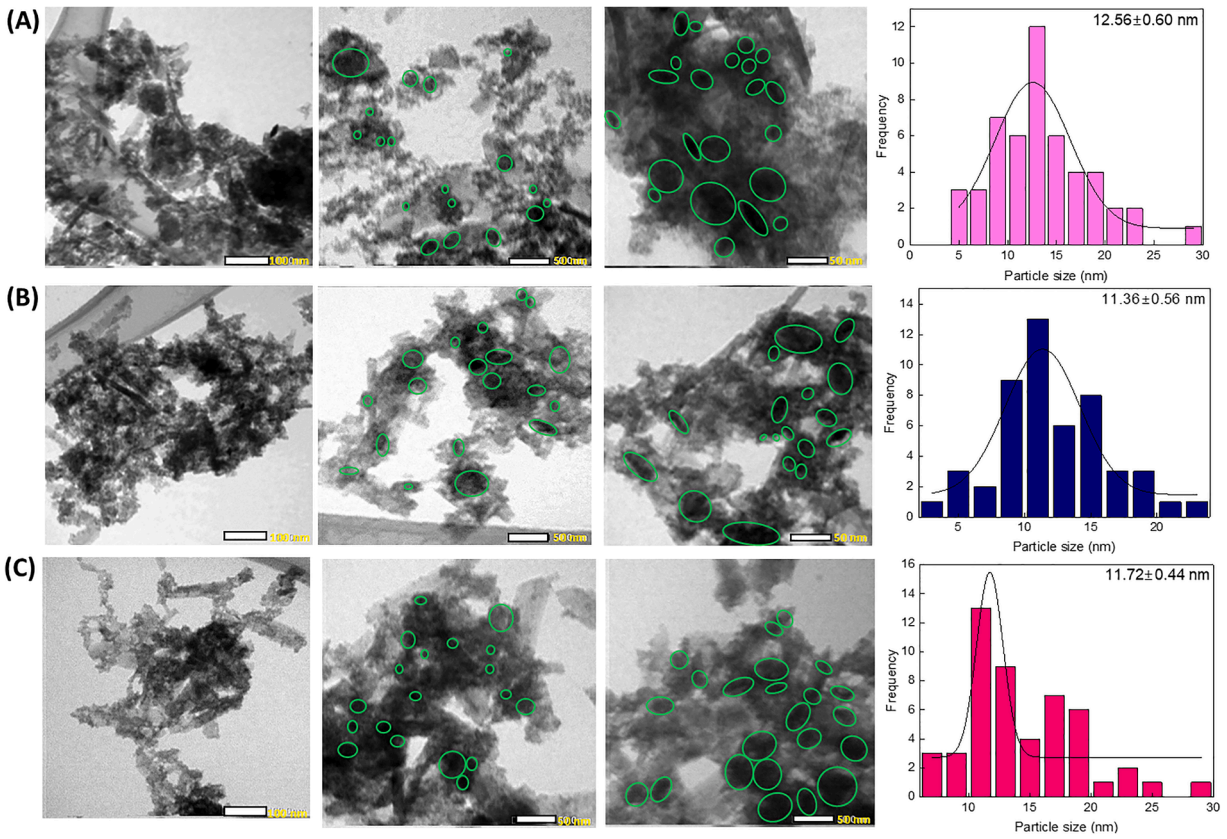

Fig. 9. TEM micrographs of polymer-capped IONP (A) IONP-PEG, (B) IONP-PVP, and (C) IONP-HPMC. The green circle indicates the IONP core.

cluster; meanwhile, the PEG and PVP at all concentrations, followed by HPMC-capped IONP at low to moderate concentrations, constructed a cluster together, indicating similar physicochemical properties and antibacterial activity. Meanwhile, these polymer-capped IONP presented a distinct cluster compared to the bare IONP, suggesting the successful performance of the capping layer to alter the physicochemical properties of IONP. Notably, the HPMC-capped IONP at 1.0% concentrations observed as a separate cluster, implicating that the high concentrations of HPMC formed a particular behavior. This is presumably due to excellent steric stabilization that provoked a smaller particle size, enhanced band gap energy, and outstanding inhibition zone diameter for antibacterial activity. The loading plots further emphasized the contribution of each variable to the principal component. The vectors of hydrodynamic particle size and zeta potential were aligned closely, indicating a similar pattern of these variables on the principal components. Meanwhile, the directions of the hydrodynamic particle size, zeta potential, and PDI variables were observed opposite to the inhibition zone, implying the inverse relationship between particle size-related properties and antibacterial activity. The magnetization value and band gap energy constructed a separate vector group, indicating the independent character of these variables as physicochemical properties that are essential for determining the effect of the polymer as a capping layer. Therefore, the combination of particle size properties, magnetization, and electronic properties was adequate to capture the excellent system of polymer-capped IONP produced in this study. Herein, IONP-PEG 1.0%, IONP-PVP 0.1%, and IONP-HPMC 1.0% were pointed out as the promising systems due to the higher vector length of the first component among the other concentrations for each polymer. In summary, the escalation of PEG and HPMC concentration as a capping layer contributed to the reduction of hydrodynamic particle size, increment of band gap energy, and magnetization. Consequently, the enhancement of antibacterial activity was observed for those systems due to easier interaction with the bacterial cell wall [57]. Meanwhile, the increment of PVP concentration as a capping layer reduced the antibacterial activity of IONP. This is probably due to a larger hydrodynamic particle size, followed by smaller magnetization and band gap energy [98]. Thus, the inhibition capacity of PVP-capped IONP towards bacteria was decreased along with the increase in polymer concentration as a capping layer.

3.9. Transmission electron microscopy (TEM) analysis

The most promising systems of polymer-capped IONP determined by PCA analysis, herein IONP-PEG 1.0%, IONP-PVP 0.1%, and IONP-HPMC 1.0%, were further analyzed using transmission electron microscopy (TEM) analysis to confirm the morphological state and IONP particle size. The TEM images depicted in Fig. 9 presented the nearly spherical and elliptical shape of the IONP core (darker site), distributed in a sheet-like structure of polymer as a capping layer (lighter site). The inorganic IONP core determined from the promising systems of polymer-capped IONP ranged between 11.36±0.56 nm and 12.56±0.60 nm, followed by a narrow size distribution. These results are in line with the previous development of oleic acid-capped IONP that exhibited IONP core diameters in the range of 6.15 ± 0.98 and 17.6 ± 0.91 nm [10]. TEM results confirm that capping layers enclosed the IONP core and hindered the formation of larger IONP aggregates. The particle size determined from TEM images presented a lower value than the hydrodynamic particle size and SEM-derived particle size, since this method measured the in situ core size of IONP [106]. Furthermore, the type of capping layer also produced distinct behavior of the IONP core on the polymer-capped IONP structure. PVP exhibited strong surface functionalization and a narrower particle-size distribution due to intensive interactions, while PEG showed moderate steric stabilization. HPMC possessed polymer entanglement due to the highest molecular weight and bulky structure at 1.0% concentration [104].

Compared with PSA results, the particle size determined by TEM analysis showed a similar trend to the hydrodynamic particle size measured by PSA. IONP-PVP 0.1% exhibited the smallest particle size, followed by IONP-HPMC 1.0% and IONP-PEG 1.0%,

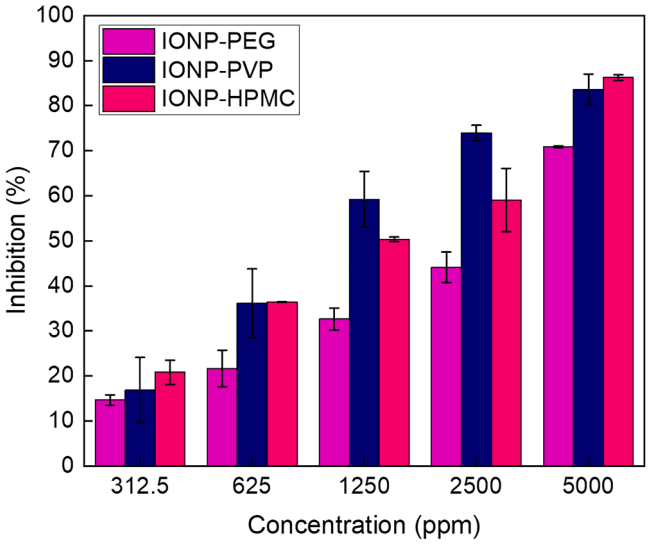

Fig. 10. ROS scavenging activity profile of selected polymer-capped IONP.

respectively. A similar particle size trend of the polymer-capped IONP was observed by TEM analysis and PSA, explaining the correlation between colloidal state and dry state particle size determination. These results also confirmed the capability of the polymer to inhibit IONP core agglomeration and enclose the surface of IONP, both in the colloidal dispersion and dry particle state.

3.10. Reactive oxygen species (ROS) scavenging activity, minimum inhibitory concentration (MIC), and minimum bactericidal concentration (MBC) analysis

The ROS scavenging activity of the selected polymer-capped IONP systems was concentration-dependent inhibition, as presented in Fig.10. The samples prepared at 5000 ppm concentration exhibited the highest inhibition percentage of radical species for all the systems. The prepared polymer-capped IONP showed inhibition activity of 70.85%, 83.58%, and 86.24% for PEG, PVP, and HPMC-capped IONP, respectively. The inhibition activity of IONP-PVP 0.1% and IONP-HPMC 1.0% was higher than the inhibition activity of vitamin C as a positive control, which exhibited 72.11% inhibition. A similar observation was reported by Sulaiman *et al.*, which presented high free radical scavenging activity of about 76.3% [107]. The confirmed radical scavenging activity of the polymer-capped IONP explained its advantages in preserving biological systems and the non-toxic properties of specific delivery [107]. The radical scavenging activity of the polymer-capped IONP resulted from the synergism of the IONP core and the surface coating of polymers. However, this result also confirmed that the antibacterial mechanism of the prepared polymer-capped IONP in this study was not primarily directed through ROS production mechanisms, but also supported by other mechanisms such as physical and electrostatic interactions that disrupted the bacterial cell membrane [108].

The determination of the MIC and MBC of polymer-capped IONP against *Escherichia coli* and *Staphylococcus aureus* showed no inhibitory or bactericidal activity up to 5000 ppm of the samples, as arranged. These results explained the limited efficacy of the broth-based system method in elaborating the antibacterial potency of polymer-capped IONP due to poor dispersion of these nanoparticles in liquid growth medium and turbid consistency of the dispersion, which affected the endpoint determination of bacterial growth [109]. In the microbroth dilution method, high concentrations of electrolytes and salts can interfere with the surface charge of nanoparticles, inducing particle aggregation and sedimentation at the bottom of the well. Hence, limiting polymer-capped IONP contact with bacterial cell membranes [110]. In contrast, the disc diffusion assay demonstrated an inhibition zone, confirming the ability of higher localized concentrations of polymer-capped IONP to inhibit bacterial growth. These results confirmed that zeta potential and electrostatic surface charge of the prepared IONP predominantly influenced antibacterial activity through direct physical contact [110, 111]. The antibacterial effect displayed in the disc diffusion method is generally mediated by intracellular ROS generation and electrostatic interaction leading to membrane damage, whereas the MIC/MBC assays described the limitations of nanoparticle dispersion and coating-mediated ROS production in aqueous media [112]. Further studies are required using a wider range of polymer-capped IONP concentrations to determine the MIC value of this system. However, the potential radical scavenging activity of polymer-capped IONP supports their multifunctional potential as antibacterial agents and antioxidants in the biomedical field.

4. Conclusion

The application of a polymer as a capping layer could improve the physicochemical properties of IONP, as well as their colloidal dispersion. Three different hydrophilic polymers, including PEG (PEG 4000), PVP (PVP K-30), and HPMC (HPMC E15), were successfully employed in this study to produce a smaller and more uniform dispersion of IONP. The results of SEM-EDX and TEM analysis also revealed the capability of these polymers to cover the surface of the bare IONP, which is mainly constructed through hydrogen bond interaction as presented in the FT-IR spectrum. The result of PCA analysis revealed that the increment of PEG and HPMC from 0.1% to 1.0% concentrations resulted in a smaller particle size, higher band gap energy, enhancement of magnetization value, and higher inhibition zone diameter towards *Staphylococcus aureus* and *Esherichia coli*. In contrast, the higher concentration of PVP as a capping layer produced a larger particle size, lower band gap energy, and a reduction of magnetization value, in conjunction with its lower inhibition zone diameter. The promising polymer-capped IONP systems for further development were IONP-PEG 1.0%, IONP-PVP 0.1%, and IONP-HPMC 1.0%, as depicted through PCA analysis. The MIC and MBC analysis using the microbroth dilution method revealed no antibacterial inhibition until a 5000-ppm concentration of the promising polymer capped-IONP due to limited direct contact with the bacterial cell membrane in aqueous medium. Meanwhile, the disk diffusion assay of antibacterial activity showed an inhibition zone diameter, suggesting the moderate potency of localized contact of polymer-capped-IONP in inhibiting bacterial growth. Further investigations using a wider range of polymer-capped IONP concentrations should be conducted to investigate the antibacterial activity of the polymer-capped-IONP. However, these systems also performed ROS scavenging activity, confirming their potential properties for antibacterial and antioxidant purposes.

CRediT authorship contribution statement

Karina Citra Rani: Writing – original draft, Visualization, Methodology, Investigation, Data curation, Conceptualization. **Agnes Nuniek Winantari:** Writing – review & editing, Supervision, Formal analysis. **Tahta Amrillah:** Writing – review & editing, Visualization, Supervision, Software, Methodology, Formal analysis, Conceptualization. **Erizal Zaini:** Writing – review & editing, Validation, Supervision, Formal analysis. **Dwi Setyawan:** Writing – review & editing, Validation, Supervision, Methodology, Formal analysis, Conceptualization.

Declaration of competing interest

The authors declare that they have no known competing financial interests or personal relationships that could have appeared to influence the work reported in this paper.

Acknowledgment

This project is supported by the Indonesian Ministry of Finance and the Indonesian Endowment Fund for Education (LPDP) for providing financial support to this research.

Supplementary materials

Supplementary material associated with this article can be found, in the online version, at doi:10.1016/j.onano.2026.100320.

References

[1] P. Wang, S. Chai, Y. Zhang, X. Wang, W. Pei, L. Zheng, Z. Xu, Q. Jiang, N. Gu, J. Sun, Knowledge mining inspired therapy of osteoporosis by magnetic hydrogel mediated precise stimulation of vagus nerve under a rotational magnetic field, Nano Res. 18 (2024) 94907503, https://doi.org/10.26599/NR.2025.94907503.
[2] Q. Wang, K. Feng, G. Wan, W. Liao, J. Jin, P. Wang, X. Sun, W. Wang, Q. Jiang, A ROS-responsive hydrogel encapsulated with matrix metalloproteinase-13 siRNA nanocarriers to attenuate osteoarthritis progression, J. Nanobiotechnol. 23 (2025) 18, https://doi.org/10.1186/s12951-024-03046-7.
[3] Q. Wang, L. Wang, X. Liu, H. Chen, X. Wang, P. Wang, W. Wang, Q. Jiang, A pH-responsive magnetic-controlled nanocomposite for precise and efficient vancomycin delivery in treating prosthetic joint infections, Adv. Compos. Hybrid. Mater. 8 (2025) 115, https://doi.org/10.1007/s42114-024-01079-y.
[4] N. Tabassum, V. Singh, V.K. Chaturvedi, E. Vamanu, M.P. Singh, A facile synthesis of flower-like iron oxide nanoparticles and its efficacy measurements for antibacterial, cytotoxicity and antioxidant activity, Pharmaceutics 15 (2023) 1726, https://doi.org/10.3390/pharmaceutics15061726.
[5] S. Das, S. Diyali, G. Vinothini, B. Perumalsamy, G. Balakrishnan, T. Ramasamy, D. Dharumadurai, B. Biswas, Synthesis, morphological analysis, antibacterial activity of iron oxide nanoparticles and the cytotoxic effect on lung cancer cell line, Heliyon 6 (2020) e04953, https://doi.org/10.1016/j.heliyon.2020.e04953.
[6] S. Vihodceva, A. Šutka, M. Sihtmäe, M. Rosenberg, M. Otsus, I. Kurvet, K. Smits, L. Bikse, A. Kahru, K. Kasemets, Antibacterial activity of positively and negatively charged hematite (α-Fe2O3) nanoparticles to *E. coli*, Staphylococcus aureus and vibrio fischeri, Nanomaterials 11 (2021) 652, https://doi.org/10.3390/nano11030652.
[7] S.V. Gudkov, D.E. Burmistrov, D.A. Serov, M.B. Rebezov, A.A. Semenova, A.B. Lisitsyn, Do iron oxide nanoparticles have significant antibacterial properties? Antibiotics 10 (2021) 884, https://doi.org/10.3390/antibiotics10070884.
[8] N. Tran, T.J. Webster, Effects of magnetite and maghemite nanoparticles on bone cell and Staphylococcus Aureus functions, Technol. Innov. 13 (2011) 39–50, https://doi.org/10.3727/194982411×13003853539876.
[9] M. Bustamante-Torres, D. Romero-Fierro, J. Estrella-Nuñez, B. Arcentales-Vera, E. Chichande-Proaño, E. Bucio, Polymeric composite of magnetite iron oxide nanoparticles and their application in biomedicine: a review, Polymers 14 (2022) 752, https://doi.org/10.3390/polym14040752.
[10] F. Ahmadpoor, A. Masood, N. Feliu, W.J. Parak, S.A. Shojaosadati, The effect of surface coating of iron oxide nanoparticles on magnetic resonance imaging relaxivity, Front. Nanotechnol. 3 (2021) 644734, https://doi.org/10.3389/fnano.2021.644734.
[11] P. Nehra, R. Chauhan, N. Garg, K. Verma, Antibacterial and antifungal activity of chitosan coated iron oxide nanoparticles, Br. J. Biomed. Sci. 75 (2018) 13–18, https://doi.org/10.1080/09674845.2017.1347362.
[12] J. Galanis, A. Sood, R. Gill, D. Harries, The contribution of capping layer dielectric properties to nanoparticle stability, Colloids Surf. A: Physicochem. Eng. Asp. 483 (2015) 239–247, https://doi.org/10.1016/j.colsurfa.2015.05.015.
[13] Y. Yang, Y. Liu, L. Song, X. Cui, J. Zhou, G. Jin, A.R. Boccaccini, S. Virtanen, Iron oxide nanoparticle-based nanocomposites in biomedical application, Trends Biotechnol. 41 (2023) 1471–1487, https://doi.org/10.1016/j.tibtech.2023.06.001.
[14] A. Rajan, M. Sharma, N.K. Sahu, Assessing magnetic and inductive thermal properties of various surfactants functionalised Fe3O4 nanoparticles for hyperthermia, Sci. Rep. 10 (2020) 15045, https://doi.org/10.1038/s41598-020-71703-6.
[15] K.C. Barick, E. Ekta, S.L. Gawali, A. Sarkar, A. Kunwar, K.I. Priyadarsini, P.A. Hassan, Pluronic stabilized Fe_3O_4 magnetic nanoparticles for intracellular delivery of curcumin, RSC Adv. 6 (2016) 98674–98681, https://doi.org/10.1039/C6RA21207G.
[16] R. Javed, M. Zia, S. Naz, S.O. Aisida, N.U. Ain, Q. Ao, Role of capping agents in the application of nanoparticles in biomedicine and environmental remediation: recent trends and future prospects, J. Nanobiotechnol. 18 (2020) 172, https://doi.org/10.1186/s12951-020-00704-4.
[17] J. Yu, R.J. Nap, I. Szleifer, J.Y. Wong, Effect of polymer surface modification of superparamagnetic iron oxide nanoparticle dispersions in high salinity environments, Langmuir. 35 (2019) 15864–15871, https://doi.org/10.1021/acs.langmuir.9b01944.
[18] G.C. Lavorato, J.C. Azcárate, M.B. Rivas Aiello, J.M. Orozco Henao, P. Mendoza Zélis, M. Ceolin, E. Winkler, M.H. Fonticelli, C. Vericat, Hydrophilization of magnetic nanoparticles with an amphiphilic polymer revisited: roles of nanoparticle capping density and polymer structure, Appl. Surf. Sci. 570 (2021) 151171, https://doi.org/10.1016/j.apsusc.2021.151171.
[19] Y. Li, N. Wang, X. Huang, F. Li, T.P. Davis, R. Qiao, D. Ling, Polymer-assisted magnetic nanoparticle assemblies for biomedical applications, ACS Appl. Bio Mater. 3 (2020) 121–142, https://doi.org/10.1021/acsabm.9b00896.
[20] M.F. Tai, C.W. Lai, S.B. Abdul Hamid, Facile synthesis polyethylene glycol coated magnetite nanoparticles for high colloidal stability, J. Nanomater. 2016 (2016) 1–7, https://doi.org/10.1155/2016/8612505.
[21] Y. Sun, X. Wang, H.L. Lee, Comprehensive investigation of solvent effects on BiOBr synthesis: understanding the photocatalytic mechanisms of enrofloxacin and its degradation pathway, Catal. Commun. 187 (2024) 106877, https://doi.org/10.1016/j.catcom.2024.106877.
[22] W. Xue, Y. Liu, N. Zhang, Y. Yao, P. Ma, H. Wen, S. Huang, Y.E. Luo, H. Fan, Effects of core size and PEG coating layer of iron oxide nanoparticles on the distribution and metabolism in mice, Int. J. Nanomed. 13 (2018) 5719–5731, https://doi.org/10.2147/IJN.S165451.
[23] A.R. Mahdavian, M.A.-S. Mirrahimi, Efficient separation of heavy metal cations by anchoring polyacrylic acid on superparamagnetic magnetite nanoparticles through surface modification, Chem. Eng. J. 159 (2010) 264–271, https://doi.org/10.1016/j.cej.2010.02.041.
[24] R.A. Bepari, P. Bharali, B.K. Das, Controlled synthesis of α- and γ-Fe2O3 nanoparticles via thermolysis of PVA gels and studies on α-Fe2O3 catalyzed styrene epoxidation, J. Saudi Chem. Soc. 21 (2017) S170–S178, https://doi.org/10.1016/j.jscs.2013.12.010.
[25] D. Bharathi, R. Ranjithkumar, S. Vasantharaj, B. Chandarshekar, V. Bhuvaneshwari, Synthesis and characterization of chitosan/iron oxide nanocomposite for biomedical applications, Int. J. Biol. Macromol. 132 (2019) 880–887, https://doi.org/10.1016/j.ijbiomac.2019.03.233.
[26] M. Madkour, A. Bumajdad, F. Al-Sagheer, To what extent do polymeric stabilizers affect nanoparticles characteristics? Adv. Colloid Interface Sci. 270 (2019) 38–53, https://doi.org/10.1016/j.cis.2019.05.004.

[27] M.M. Ali, W.S. Mahmod, A.M. Ali, Study the effect of polymers type on preparation and characterization of etoposide-loaded gold nanoparticles, Int. J. Drug Deliv. Technol. 13 (2022) 713–721, https://doi.org/10.25258/ijddt.13.2.39.

[28] N.M. Al-Hada, A.M. Al-Ghaili, H. Kasim, M.A. Saleh, M.H. Flaifel, H.M. Kamari, H. Baqiah, J. Liu, W. Jihua, The effect of PVP concentration on particle size, morphological and optical properties of cassiterite nanoparticles, IEEE Access 8 (2020) 93444–93454, https://doi.org/10.1109/ACCESS.2020.2993689.

[29] N.V. Mdlovu, F.A. Mavuso, K.-S. Lin, T.-W. Chang, Y. Chen, S.S.-S. Wang, C.-M. Wu, N.B. Mdlovu, Y.-S. Lin, Iron oxide-pluronic F127 polymer nanocomposites as carriers for a doxorubicin drug delivery system, Colloids Surf. A: Physicochem. Eng. Asp. 562 (2019) 361–369, https://doi.org/10.1016/j.colsurfa.2018.11.052.

[30] K.C. Rani, A.N. Winantari, T. Amrillah, D. Setyawan, Characterization and antibacterial activity of iron oxide nanoparticles synthesized using co-precipitation method, Chem. Phys. Impact 11 (2025) 100943, https://doi.org/10.1016/j.chphi.2025.100943.

[31] S. Schwaminger, C. Syhr, S. Berensmeier, Controlled synthesis of magnetic iron oxide nanoparticles: magnetite or maghemite? Crystals 10 (2020) 214, https://doi.org/10.3390/cryst10030214.

[32] B.H. Hui, M.N. Salimi, Production of iron oxide nanoparticles by Co-precipitation method with optimization studies of processing temperature, pH and stirring rate, Mater. Sci. Eng. (2019).

[33] K. Petcharoen, A. Sirivat, Synthesis and characterization of magnetite nanoparticles via the chemical co-precipitation method, Mater. Sci. Eng.: B 177 (2012) 421–427, https://doi.org/10.1016/j.mseb.2012.01.003.

[34] L. Rahman, S. Bhattacharjee, S. Islam, F. Zahan, B. Biswas, N. Sharmin, A study on the preparation and characterization of maghemite (γ-Fe_2O_3) particles from iron-containing waste materials, J. Asian Ceram. Soc. 8 (2020) 1083–1094, https://doi.org/10.1080/21870764.2020.1812838.

[35] I. Kumar, R. Nayak, L.B. Chaudhary, V.N. Pandey, S.K. Mishra, N.K. Singh, A. Srivastava, S. Prasad, R.M. Naik, Fabrication of α-Fe_2O_3 nanostructures: synthesis, characterization, and their promising application in the treatment of carcinoma A549 lung cancer cells, ACS Omega 7 (2022) 21882–21890, https://doi.org/10.1021/acsomega.2c02083.

[36] O. Karaagac, H. Köçkar, Improvement of the saturation magnetization of PEG coated superparamagnetic iron oxide nanoparticles, J. Magn. Magn. Mater. 551 (2022) 169140, https://doi.org/10.1016/j.jmmm.2022.169140.

[37] S.N. Che Mohamed Hussein, Z. Amir, B.M. Jan, M. Khalil, A. Azizi, Colloidal stability of CA, SDS and PVA coated iron oxide nanoparticles (IONPs): effect of molar ratio and salinity, Polymers 14 (2022) 4787, https://doi.org/10.3390/polym14214787.

[38] K.A. Mohammed, S.A. Abdulridha, E.H. Aljbory, A.H.O. Alkhayatt, R.S. Zabibah, A.J. Alrubaie, S.K. Rady, S.H. Kizar, S.S. Hariz, M.J. Kadhem, Capping agent effect on optical properties of Fe2O3 nanoparticles, Mater. Today: Proc. 56 (2022) 2010–2015, https://doi.org/10.1016/j.matpr.2021.11.346.

[39] D. Arista, A. Rachmawati, N. Ramadhani, R. Eko Saputro, A. Taufiq, Sunaryono, Antibacterial performance of Fe_3O_4 /PEG-4000 prepared by Co-precipitation route, IOP Conf. Ser.: Mater. Sci. Eng. 515 (2019) 012085, https://doi.org/10.1088/1757-899X/515/1/012085.

[40] M.A. Hoque, M.R. Ahmed, G.T. Rahman, M.T. Rahman, M.A. Islam, M.A. Khan, M.K. Hossain, Fabrication and comparative study of magnetic Fe and α-Fe2O3 nanoparticles dispersed hybrid polymer (PVA + Chitosan) novel nanocomposite film, Results Phys. 10 (2018) 434–443, https://doi.org/10.1016/j.rinp.2018.06.010.

[41] J. Yoonus, R. Resmi, B. Beena, Evaluation of antibacterial and anticancer activity of green synthesized iron oxide (α-Fe2O3) nanoparticles, Mater. Today: Proc. 46 (2021) 2969–2974, https://doi.org/10.1016/j.matpr.2020.12.426.

[42] N. Eom, M.E. Messing, J. Johansson, K. Deppert, General trends in core–shell preferences for bimetallic nanoparticles, ACS Nano 15 (2021) 8883–8895, https://doi.org/10.1021/acsnano.1c01500.

[43] R. Tantra, C. Oksel, K.N. Robinson, A. Sikora, X.Z. Wang, T.A. Wilkins, A method for assessing nanomaterial dispersion quality based on principal component analysis of particle size distribution data, Particuology 22 (2015) 30–38, https://doi.org/10.1016/j.partic.2014.10.004.

[44] F.Y. Alzoubi, O. Abu Noqta, T. Al Zoubi, H.M. Al-Khateeb, M.K. Alqadi, A. Abuelsamen, G.N. Makhadmeh, A novel one-pot synthesis of PVP-coated iron oxide nanoparticles as biocompatible contrast agents for enhanced T2-weighted MRI, J. Compos. Sci. 7 (2023) 131, https://doi.org/10.3390/jcs7030131.

[45] J.S. Nagi, K. Skorenko, W. Bernier, W.E. Jones, A.L. Doiron, Near infrared-activated dye-linked ZnO nanoparticles release reactive oxygen species for potential use in photodynamic therapy, Materials 13 (2019) 17, https://doi.org/10.3390/ma13010017.

[46] L. Yi, Y. Bai, X. Chen, W. Wang, C. Zhang, Z. Shang, Z. Zhang, J. Li, M. Cao, Z. Zhu, J. Zhang, Synergistic effects and mechanisms of action of rutin with conventional antibiotics against *E. coli*, Int. J. Mol. Sci. 25 (2024) 13684, https://doi.org/10.3390/ijms252413684.

[47] J. Sarkar, M.M.R. Mollick, D. Chattopadhyay, K. Acharya, An eco-friendly route of γ-Fe2O3 nanoparticles formation and investigation of the mechanical properties of the HPMC-γ-Fe2O3 nanocomposites, Bioprocess. Biosyst. Eng. 40 (2017) 351–359, https://doi.org/10.1007/s00449-016-1702-x.

[48] A. Bahari, Characteristics of Fe3O4, α -Fe2O3, and γ-Fe_2O_3 nanoparticles as suitable candidates in the field of nanomedicine, J. Supercond. Nov. Magn. 30 (2017) 2165–2174, https://doi.org/10.1007/s10948-017-4014-8.

[49] A. Bali Ogholbeyg, A. Kianvash, A. Hajalilou, E. Abouzari-Lotf, A. Zarebkohan, Cytotoxicity characteristics of green assisted-synthesized superparamagnetic maghemite (γ-Fe2O3) nanoparticles, J. Mater. Sci.: Mater. Electron. 29 (2018) 12135–12143, https://doi.org/10.1007/s10854-018-9321-8.

[50] M. Ebadi, A. Rifqi Md Zain, T.H. Tengku Abdul Aziz, H. Mohammadi, C.A.T. Tee, M. Rahimi Yusop, Formulation and characterization of Fe3O4@PEG nanoparticles loaded Sorafenib; molecular studies and evaluation of cytotoxicity in liver cancer cell lines, Polymers 15 (2023) 971, https://doi.org/10.3390/polym15040971.

[51] Y.-J. Song, M. Wang, X.-Y. Zhang, J.-Y. Wu, T. Zhang, Investigation on the role of the molecular weight of polyvinyl pyrrolidone in the shape control of high-yield silver nanospheres and nanowires, Nanoscale Res. Lett. 9 (2014) 17, https://doi.org/10.1186/1556-276X-9-17.

[52] C. Dong, X. Zhang, H. Cai, Green synthesis of monodisperse silver nanoparticles using hydroxy propyl methyl cellulose, J. Alloys Compd. 583 (2014) 267–271, https://doi.org/10.1016/j.jallcom.2013.08.207.

[53] R. Ianoș, E.-A. Moacă, A. Căpraru, R. Lazău, C. Păcurariu, Maghemite, γ-Fe2O3, nanoparticles preparation via carbon-templated solution combustion synthesis, Ceram. Int. 44 (2018) 14090–14094, https://doi.org/10.1016/j.ceramint.2018.04.258.

[54] S.S. Abouelkheir, H.A.H. Ibrahim, E.A. Beltagy, Functionalized maghemite superparamagnetic iron oxide nanoparticles (γ-Fe2O3-SPIONs)-amylase enzyme hybrid in biofuel production, Sci. Rep. 13 (2023) 11117, https://doi.org/10.1038/s41598-023-37826-2.

[55] O. Kvitek, E. Mutylo, B. Vokata, P. Ulbrich, D. Fajstavr, A. Reznickova, V. Svorcik, Photochemical preparation of silver colloids in hydroxypropyl methylcellulose for antibacterial materials with controlled release of silver, Coatings 10 (2020) 1046, https://doi.org/10.3390/coatings10111046.

[56] E. Gharibshahian, M. Gharibshahian, M.J. Tafreshi, M. Bahraminasab, S. Arab, The effect of capping agent on morphology, surface functionalization, and biocompatibility properties of KTiOPO4 nanoparticles, Heliyon 10 (2024) e40513, https://doi.org/10.1016/j.heliyon.2024.e40513.

[57] I.S. Okeke, K.K. Agwu, A.A. Ubachukwu, I.G. Madiba, M. Maaza, G.M. Whyte, F.I. Ezema, Impact of particle size and surface defects on antibacterial and photocatalytic activities of undoped and Mg-doped ZnO nanoparticles, biosynthesized using one-step simple process, Vacuum 187 (2021) 110110, https://doi.org/10.1016/j.vacuum.2021.110110.

[58] Y.Y. Xu, D. Zhao, X.J. Zhang, W.T. Jin, P. Kashkarov, H. Zhang, Synthesis and characterization of single-crystalline α-Fe2O3 nanoleaves, Physica E: low-dimensional systems and, Nanostructures 41 (2009) 806–811, https://doi.org/10.1016/j.physe.2008.12.015.

[59] T.M.D. Dang, T.T.T. Le, E. Fribourg-Blanc, M.C. Dang, Synthesis and optical properties of copper nanoparticles prepared by a chemical reduction method, Adv. Nat. Sci: Nanosci. Nanotechnol. 2 (2011) 015009, https://doi.org/10.1088/2043-6262/2/1/015009.

[60] K.H. Kim, R. Bhujel, R. Maharjan, J.C. Lee, H.S. Jung, H.J. Kim, N.A. Kim, S.H. Jeong, Biophysical characterization of siRNA-loaded lipid nanoparticles with different PEG content in an aqueous system, Eur. J. Pharm. Biopharm. 190 (2023) 150–160, https://doi.org/10.1016/j.ejpb.2023.07.013.

[61] L.V. Borkovska, O. Gudymenko, O. Stroyuk, A. Raevskaya, O. Fesenko, T. Kryshtab, 1 V. Lashkaryov Institute of Semiconductor Physics of National Academy of Sciences (NAS) of Ukraine, 41 Pr. Nauky, 03028 Kyiv, Ukraine, photoinduced transformations of optical properties of CdSe and Ag-In-S nanocrystals embedded in the films of polyvinyl alcohol, AIMS Mater. Sci. 3 (2016) 658–668, https://doi.org/10.3934/matersci.2016.2.658.

[62] D.C. Deka, A. Kalita, S. Bardaloi, M.P.C. Kalita, Influence of capping agent on structural, optical and photocatalytic properties of ZnS nanocrystals, J. Lumin. 210 (2019) 269–275, https://doi.org/10.1016/j.jlumin.2019.02.033.

[63] A. Rónavári, P. Bélteky, E. Boka, D. Zakupszky, N. Igaz, B. Szerencsés, I. Pfeiffer, Z. Kónya, M. Kiricsi, Polyvinyl-pyrrolidone-coated silver nanoparticles—the colloidal, chemical, and biological consequences of steric stabilization under biorelevant conditions, Int. J. Mol. Sci. 22 (2021) 8673, https://doi.org/10.3390/ijms22168673.

[64] M.F. Tai, C.W. Lai, S.B. Abdul Hamid, Facile synthesis polyethylene glycol coated magnetite nanoparticles for high colloidal stability, J. Nanomater. 2016 (2016) 1–7, https://doi.org/10.1155/2016/8612505.

[65] B. Biswas, M.L. Rahman, M.F. Ahmed, N. Sharmin, Extraction of gamma iron oxide (γ-Fe2O3) nanoparticles from waste can: structure, morphology and magnetic properties, Heliyon 10 (2024) e30810, https://doi.org/10.1016/j.heliyon.2024.e30810.

[66] Z. Wei, C. Wang, S. Zou, H. Liu, Z. Tong, Fe2O3 nanoparticles as particulate emulsifier: preparation of magnetic and biocompatible PLGA microcapsules, Colloids Surf. A: Physicochem. Eng. Asp. 392 (2011) 116–123, https://doi.org/10.1016/j.colsurfa.2011.09.043.

[67] P. Wang, J. Fang, S. Qin, Y. Kang, D.-M. Zhu, Molecular weight dependence of viscosity and shear modulus of polyethylene glycol (PEG) solution boundary layers, J. Phys. Chem. C 113 (2009) 13793–13800, https://doi.org/10.1021/jp903060q.

[68] J.-N. Sun, Y. Hu, W.E. Frieze, W. Chen, D.W. Gidley, How pore size and surface roughness affect diffusion barrier continuity on porous low-k films, J. Electrochem. Soc. 150 (2003) F97, https://doi.org/10.1149/1.1565140.

[69] L.M. Mason, M.D. Campiñez, S.R. Pygall, J.C. Burley, P. Gupta, D.E. Storey, I. Caraballo, C.D. Melia, The influence of polymer content on early gel-layer formation in HPMC matrices: the use of CLSM visualisation to identify the percolation threshold, Eur. J. Pharm. Biopharm. 94 (2015) 485–492, https://doi.org/10.1016/j.ejpb.2015.06.019.

[70] K. Kathiresan, S. Durairaj, Green synthesis of iron oxide nanoparticles using date seed extracts for biomedical applications, Int. J. Env. Sci. Technol. 22 (2025) 15167–15188, https://doi.org/10.1007/s13762-025-06585-0.

[71] P. Kaur, M.S. Bakshi, Block polymer-functionalized iron oxide nanoparticles for the solid–liquid interfacial extraction of industrial dyes: sustainable methodology based on molecular interactions, ACS Appl. Polym. Mater. 6 (2024) 8659–8670, https://doi.org/10.1021/acsapm.4c01751.

[72] R. Kol, T. De Somer, D.R. D'hooge, F. Knappich, K. Ragaert, D.S. Achilias, S. De Meester, State-of-the-art quantification of polymer solution viscosity for plastic waste recycling, ChemSusChem 14 (2021) 4071–4102, https://doi.org/10.1002/cssc.202100876.

[73] F. Baldassarre, M. Cacciola, G. Ciccarella, A predictive model of iron oxide nanoparticles flocculation tuning Z-potential in aqueous environment for biological application, J. NanoPart Res. 17 (2015) 377, https://doi.org/10.1007/s11051-015-3163-6.

[74] S. Buratto, E. Latocheski, D. De Oliveira, J. Domingos, Influence of the capping agent PVP of the outer layer of Pd nanocubes surface on the catalytic hydrogenation of unsaturated C−C bonds, J. Braz. Chem. Soc. (2020), https://doi.org/10.21577/0103-5053.20190250.

[75] R. Zein, I. Alghoraibi, C. Soukkarieh, M.T. Ismail, A. Alahmad, Influence of polyvinylpyrrolidone concentration on properties and anti-bacterial activity of green synthesized silver nanoparticles, Micromachines 13 (2022) 777, https://doi.org/10.3390/mi13050777.

[76] Z. Jiang, X. Bai, Effects of polysaccharide concentrations on the formation and physical properties of emulsion-templated oleogels, Molecules 27 (2022) 5391, https://doi.org/10.3390/molecules27175391.

[77] F.M. Abdulsada, N.N. Hussein, G.M. Sulaiman, A. Al Ali, M. Alhujaily, Evaluation of the antibacterial properties of iron oxide, polyethylene glycol, and gentamicin conjugated nanoparticles against some multidrug-resistant bacteria, J. Funct. Biomater. 13 (2022) 138, https://doi.org/10.3390/jfb13030138.

[78] A.H. Rezayan, M. Mousavi, S. Kheirjou, G. Amoabediny, M.S. Ardestani, J. Mohammadnejad, Monodisperse magnetite (Fe3O4) nanoparticles modified with water soluble polymers for the diagnosis of breast cancer by MRI method, J. Magn. Magn. Mater. 420 (2016) 210–217, https://doi.org/10.1016/j.jmmm.2016.07.003.

[79] M. Arakha, S. Pal, D. Samantarrai, T.K. Panigrahi, B.C. Mallick, K. Pramanik, B. Mallick, S. Jha, Antimicrobial activity of iron oxide nanoparticle upon modulation of nanoparticle-bacteria interface, Sci. Rep. 5 (2015) 14813, https://doi.org/10.1038/srep14813.

[80] K. Hayashi, H. Tomonaga, T. Matsuyama, J. Ida, Facile synthesis, characterization of various polymer immobilized on magnetite nanoparticles applying the coprecipitation method, J. Appl. Polym. Sci 139 (2022) 51581, https://doi.org/10.1002/app.51581.

[81] A. Sha, H. Yang, Z. He, Q. Zuo, Z. Xu, C. Wu, M. Wu, R. Chi, Mechanisms of swelling inhibition and seepage promotion of weathered crust elution-deposited rare earth ore by hydroxypropyl methyl cellulose, Miner. Eng. 202 (2023) 108213, https://doi.org/10.1016/j.mineng.2023.108213.

[82] G. Kurlyandskaya, L. Litvinova, A. Safronov, V. Schupletsova, I. Tyukova, O. Khaziakhmatova, G. Slepchenko, K. Yurova, E. Cherempey, N. Kulesh, R. Andrade, I. Beketov, I. Khlusov, Water-based suspensions of iron oxide nanoparticles with electrostatic or steric stabilization by Chitosan: fabrication, characterization and biocompatibility, Sensors 17 (2017) 2605, https://doi.org/10.3390/s17112605.

[83] S.N. Che Mohamed Hussein, Z. Amir, B.M. Jan, M. Khalil, A. Azizi, Colloidal stability of CA, SDS and PVA coated iron oxide nanoparticles (IONPs): effect of molar ratio and salinity, Polymers 14 (2022) 4787, https://doi.org/10.3390/polym14214787.

[84] B.D. Plouffe, S.K. Murthy, L.H. Lewis, Fundamentals and application of magnetic particles in cell isolation and enrichment: a review, Rep. Prog. Phys. 78 (2015) 016601, https://doi.org/10.1088/0034-4885/78/1/016601.

[85] A. Kolhatkar, A. Jamison, D. Litvinov, R. Willson, T. Lee, Tuning the magnetic properties of nanoparticles, IJMS 14 (2013) 15977–16009, https://doi.org/10.3390/ijms140815977.

[86] A.S. Teja, P.-Y. Koh, Synthesis, properties, and applications of magnetic iron oxide nanoparticles, Prog. Cryst. Growth Charact. Mater. 55 (2009) 22–45, https://doi.org/10.1016/j.pcrysgrow.2008.08.003.

[87] V. Patsula, M. Moskvin, S. Dutz, D. Horák, Size-dependent magnetic properties of iron oxide nanoparticles, J. Phys. Chem. Solids 88 (2016) 24–30, https://doi.org/10.1016/j.jpcs.2015.09.008.

[88] M. Abdolrahimi, M. Vasilakaki, S. Slimani, N. Ntallis, G. Varvaro, S. Laureti, C. Meneghini, K.N. Trohidou, D. Fiorani, D. Peddis, Magnetism of nanoparticles: effect of the organic coating, Nanomaterials 11 (2021) 1787, https://doi.org/10.3390/nano11071787.

[89] B. Andrzejewski, W. Bednarski, M. Kaźmierczak, A. Łapiński, K. Pogorzelec-Glaser, B. Hilczer, S. Jurga, G. Nowaczyk, K. Załęski, M. Matczak, B. Łęska, R. Pankiewicz, L. Kępiński, Magnetization enhancement in magnetite nanoparticles capped with alginic acid, Compos. B: Eng. 64 (2014) 147–154, https://doi.org/10.1016/j.compositesb.2014.04.022.

[90] L. Gabrielyan, A. Hovhannisyan, V. Gevorgyan, M. Ananyan, A. Trchounian, Antibacterial effects of iron oxide (Fe3O4) nanoparticles: distinguishing concentration-dependent effects with different bacterial cells growth and membrane-associated mechanisms, Appl. Microbiol. Biotechnol. 103 (2019) 2773–2782, https://doi.org/10.1007/s00253-019-09653-x.

[91] N. Lal, M. Seifan, A. Ebrahiminezhad, A. Berenjian, The effect of iron oxide nanoparticles on the menaquinone-7 isomer composition and synthesis of the biologically significant all-trans isomer, Nanomaterials 13 (2023) 1825, https://doi.org/10.3390/nano13121825.

[92] D. Ranmadugala, A. Ebrahiminezhad, M. Manley-Harris, Y. Ghasemi, A. Berenjian, Magnetic immobilization of bacteria using iron oxide nanoparticles, Biotechnol. Lett. 40 (2018) 237–248, https://doi.org/10.1007/s10529-017-2477-0.

[93] T.J. Silhavy, D. Kahne, S. Walker, The bacterial cell envelope, Cold Spring Harb. Perspect. Biol. 2 (2010) a000414, https://doi.org/10.1101/cshperspect.a000414 a000414–a000414.

[94] D. Aksu Demirezen, Ş. Yılmaz, D. Demirezen Yılmaz, Y.Ş. Yıldız, Green synthesis of iron oxide nanoparticles using *Ceratonia siliqua L.* aqueous extract: improvement of colloidal stability by optimizing synthesis parameters, and evaluation of antibacterial activity against gram-positive and gram-negative bacteria, Int. J. Mater. Res. 113 (2022) 849–861, https://doi.org/10.1515/ijmr-2022-0037.

[95] R. Prucek, J. Tuček, M. Kilianová, A. Panáček, L. Kvítek, J. Filip, M. Kolář, K. Tománková, R. Zbořil, The targeted antibacterial and antifungal properties of magnetic nanocomposite of iron oxide and silver nanoparticles, Biomaterials 32 (2011) 4704–4713, https://doi.org/10.1016/j.biomaterials.2011.03.039.

[96] M.J. Wilhelm, M. Sharifian Gh, T. Wu, Y. Li, C.-M. Chang, J. Ma, H.-L. Dai, Determination of bacterial surface charge density via saturation of adsorbed ions, Biophys. J. 120 (2021) 2461–2470, https://doi.org/10.1016/j.bpj.2021.04.018.

[97] B.M. Geilich, I. Gelfat, S. Sridhar, A.L. Van De Ven, T.J. Webster, Superparamagnetic iron oxide-encapsulating polymersome nanocarriers for biofilm eradication, Biomaterials 119 (2017) 78–85, https://doi.org/10.1016/j.biomaterials.2016.12.011.

[98] K.N. Shoudho, S. Uddin, M.M.H. Rumon, M.S. Shakil, Influence of physicochemical properties of iron oxide nanoparticles on their antibacterial activity, ACS Omega 9 (2024) 33303–33334, https://doi.org/10.1021/acsomega.4c02822.

[99] T.-G. Zhang, C.-Y. Miao, Iron oxide nanoparticles as promising antibacterial agents of new generation, Nanomaterials 14 (2024) 1311, https://doi.org/10.3390/nano14151311.
[100] S. Faisal, S. Sadiq, M. Mustafa, M.H. Khan, M. Sadiq, Z. Iqbal, M. Khan, Tailoring the antibacterial and antioxidant activities of iron nanoparticles with amino benzoic acid, RSC Sustain. 1 (2023) 139–146, https://doi.org/10.1039/D2SU00044J.
[101] M.A. Abid, D.A. Kadhim, Synthesis of iron oxide nanoparticles by mixing chilli with rust iron extract to examine antibacterial activity, Mater. Technol. 37 (2022) 1494–1503, https://doi.org/10.1080/10667857.2021.1959189.
[102] A. Alnehia, M. Hadi, H. Alnahari, A. Al-Sharabi, Optical, structural and antibacterial properties of phase heterostructured Fe2O3–CuO–CuFe2O4 nanocomposite, Sci. Rep. 14 (2024) 14392, https://doi.org/10.1038/s41598-024-64090-9.
[103] F.A.-Z. Sayed, N.G. Eissa, Y. Shen, D.A. Hunstad, K.L. Wooley, M. Elsabahy, Morphologic design of nanostructures for enhanced antimicrobial activity, J. Nanobiotechnol. 20 (2022) 536, https://doi.org/10.1186/s12951-022-01733-x.
[104] A. Filimon, M.D. Onofrei, A. Bargan, I. Stoica, S. Dunca, Bioactive materials based on hydroxypropyl methylcellulose and silver nanoparticles: structural-morphological characterization and antimicrobial testing, Polymers 15 (2023) 1625, https://doi.org/10.3390/polym15071625.
[105] J.C. Martínez, N.A. Chequer, J.L. González, T. Cordova, Alternative metodology for gold nanoparticles diameter characterization using PCA technique and UV-VIS spectrophotometry, Nanosci. Nanotechnol. 2 (2013) 184–189, https://doi.org/10.5923/j.nn.20120206.06.
[106] Y. Piñeiro-Redondo, M. Bañobre-López, I. Pardiñas-Blanco, G. Goya, M.A. López-Quintela, J. Rivas, The influence of colloidal parameters on the specific power absorption of PAA-coated magnetite nanoparticles, Nanoscale Res. Lett. 6 (2011) 383, https://doi.org/10.1186/1556-276X-6-383.
[107] G.M. Sulaiman, A.T. Tawfeeq, A.S. Naji, Biosynthesis, characterization of magnetic iron oxide nanoparticles and evaluations of the cytotoxicity and DNA damage of human breast carcinoma cell lines, Artif. Cells Nanomed. Biotechnol. 46 (2018) 1215–1229, https://doi.org/10.1080/21691401.2017.1366335.
[108] R. Shanmugam, M. Tharani, S.S. Abullais, S.R. Patil, M.I. Karobari, Black seed assisted synthesis, characterization, free radical scavenging, antimicrobial and anti-inflammatory activity of iron oxide nanoparticles, BMC Complement. Med. Ther. 24 (2024) 241, https://doi.org/10.1186/s12906-024-04552-9.
[109] M. Bubonja-Šonje, S. Knežević, M. Abram, Challenges to antimicrobial susceptibility testing of plant-derived polyphenolic compounds, Arch. Ind. Hyg. Toxicol. 71 (2020) 300–311, https://doi.org/10.2478/aiht-2020-71-3396.
[110] E. Chung, G. Ren, I. Johnston, R.K. Matharu, L. Ciric, A. Walecka, Y.-K. Cheong, Applied methods to assess the antimicrobial activity of metallic-based nanoparticles, Bioengineering 10 (2023) 1259, https://doi.org/10.3390/bioengineering10111259.
[111] A. Carrapiço, M. Pico, E.P. Carreiro, P. Barrulas, J. Mirão, A.T. Caldeira, J. Teixeira, L. Dias, M.R. Martins, Biosynthesis of silver-based nanoparticles: critical assessment of antimicrobial assays and diffusion kinetics analysis, Int. Biodeterior. Biodegrad. 205 (2025) 106167, https://doi.org/10.1016/j.ibiod.2025.106167.
[112] M. Huang, Q. Li, H. Du, Heme-loaded iron oxide nanoparticles synergistically eradicate Staphylococcus aureus Persister cells via activating Persister metabolism and Fenton reaction, Mater. Lett. 412 (2026) 140388, https://doi.org/10.1016/j.matlet.2026.140388.